Microbial signals and lymphotoxin drive TNF-independent death of A20 and ABIN-1 deficient epithelium

Running Title: A20 and ABIN-1 restrict TNF-independent death

Iulia Rusu[1*], Elvira Mennillo[1*], Zhongmei Li[1,2], Jared L. Bain[1], Xiaofei Sun[1], Kimberly Ly[3], Yenny Y. Rosli[1], Mohammad Naser[4], Zunqiu Wang[1], Rommel Advincula[1], Philip Achacoso[1], Ling Shao[5], Bahram Razani[6], Ophir D. Klein[7], Alexander Marson[1,2,3,8,9,10], Jessie A. Turnbaugh[3], Peter J. Turnbaugh[3], Barbara A. Malynn[1], Averil Ma[1#], and Michael G. Kattah[1#]

1. Department of Medicine, University of California San Francisco, San Francisco, CA, USA

2. Gladstone Institutes, San Francisco, CA, USA

3. Department of Microbiology and Immunology, University of California San Francisco, San Francisco, CA, USA

4. Biological Imaging Development CoLab, University of California San Francisco, San Francisco, CA, USA

5. Department of Medicine, University of Southern California, Los Angeles, CA, USA

6. Department of Dermatology, University of California San Francisco, San Francisco, CA, USA

7. Departments of Orofacial Sciences and Pediatrics, Program in Craniofacial Biology, and Institute for Human Genetics, University of California San Francisco, California, USA

8. Innovative Genomics Institute, University of California, Berkeley, CA

9. Parker Institute for Cancer Immunotherapy, San Francisco, CA

10. Chan Zuckerberg Biohub, San Francisco, CA

*Co-first author

To whom correspondence should be addressed:

University of California San Francisco, 513 Parnassus Ave, S-357G, San Francisco, CA 94143-0451. EM: averil.ma@ucsf.edu, michael.kattah@ucsf.edu

ABSTRACT

Anti-TNF antibodies are effective for treating patients with inflammatory bowel disease (IBD), but many patients fail to respond to anti-TNF therapy, highlighting the importance of TNF-independent disease. We previously demonstrated that acute deletion of two IBD susceptibility genes, *A20* (*Tnfaip3*) and *Abin-1* (*Tnip1*), in intestinal epithelial cells (IECs) sensitizes mice to both TNF-dependent and TNF-independent death. Here we show that TNF-independent IEC death after *A20* and *Abin-1* deletion is rescued by germ-free derivation or deletion of *MyD88*, while deletion of *Trif* provides only partial protection. Combined deletion of *Ripk3* and *Casp8*, which inhibits both apoptotic and necroptotic death, completely protects against death after acute deletion of *A20* and *Abin-1* in IECs. *A20* and *Abin-1*-deficient IECs are sensitized to TNF-independent, TNFR-1-mediated death in response to lymphotoxin alpha (LTα) homotrimers. Blockade of LTα *in vivo* reduces weight loss and improves survival when combined with partial deletion of *MyD88*. These data show that microbial signals, *MyD88*, and LTα all contribute to TNF-independent intestinal injury.

SUMMARY

Here we show that germ-free derivation, MyD88 deletion, combined Ripk3 and Casp8 deletion, or anti-LTα, all reduce TNF-independent intestinal injury after *A20* and *Abin-1* deletion.

2

INTRODUCTION

The intestinal epithelium, a single-cell layer protective lining, is critically important for preventing inflammatory responses to a vast array of microbial stimuli. Inflammatory bowel disease (IBD) is the result of an abnormal immune response to microbial stimuli in genetically susceptible individuals, culminating in intestinal epithelial cell (IEC) injury (1–6). IECs play a central role in IBD pathogenesis, and many candidate IBD-associated genes influence IEC biology, including *ITLN1*, *NOS2, ATG16L1*, *XBP1*, *A20* (*TNFAIP3*), *ABIN-1* (*TNIP1*), among others (7–12). Understanding the genetic, microbial, and environmental factors that influence IEC death and injury may enable identification of biomarkers for precision medicine and highlight novel pathways that could be targeted for treating patients with IBD.

Polymorphisms in *A20* (*TNFAIP3*) and *ABIN-1* (*TNIP1*) are linked to a variety of inflammatory disorders affecting multiple tissues, including IBD (13–17). Germline mutations causing *A20* haploinsufficiency have been identified in patients with a systemic inflammatory disorder characterized in part by intestinal ulcerations, typically with pediatric or even infantile onset (18–21). A20 and ABIN-1 are ubiquitin interacting proteins that interact with each other at the protein level, and both restrict cell death as well as NF-κB signaling downstream of TNF and Toll-like receptors (TLRs) (22–37). A20 and ABIN-1 are both expressed in human and murine intestinal epithelium. Mice with *A20*-deficient IECs develop normally, but are more susceptible to dextran sodium sulfate (DSS)-induced colitis as well as cancer induced by A20-deficient myeloid cells or collaborating oncogenes (38–40). A20 and ABIN-1 have important roles in restricting inflammation in multiple tissue types, but much remains to be learned about the role of A20 and ABIN-1 specifically in intestinal epithelial tissue damage.

We previously demonstrated that (IEC)-specific deletion of either *A20* or *Abin-1* alone does not lead to overt weight loss or intestinal injury, but acute simultaneous deletion of both *A20* and *Abin-1* leads to spontaneous IEC apoptosis, fulminant enterocolitis, and rapid mouse lethality (9). In this setting, *A20* and *Abin-1* cooperatively restrict both TNF-dependent and TNF-independent IEC death. TNF-independent IEC death is substantially less well-characterized than TNF-dependent death, and can involve microbial signals, *Trif* (*Ticam1*), *Zbp1*, interferon signaling, ripoptosome activation, or other inflammatory death pathways (41–46).

3

Anti-TNF therapy remains one of the most effective approaches for treating Crohn's disease (CD) and ulcerative colitis (UC), but roughly one-third of patients have no response and one-third of patients lose response over time (47–50). Therefore, understanding the gene products that control TNF-independent IEC injury could have significant translational relevance for anti-TNF non-responders. To better understand the pathways leading to TNF-independent IEC injury we performed *in vivo* and *in vitro* analysis of IECs after acute simultaneous deletion of *A20* and *Abin-1*.

RESULTS

Germ-free *A20/Abin-1*$^{T-\Delta IEC}$*Tnf*$^{-/-}$ mice are protected from TNF-independent IEC death

Mice with floxed A20 (*A20*$^{fl/fl}$) and floxed Abin-1 (*Abin-1*$^{fl/fl}$) on a *Vil-cre-ER*$^{T2+}$ background (*A20/Abin-1*$^{T-\Delta IEC}$) undergo acute deletion of *A20* and *Abin-1* in IECs upon treatment with tamoxifen, culminating in spontaneous apoptotic IEC death, severe enterocolitis, and rapid mouse lethality (9). This death occurs on a *Tnf*$^{+/+}$ or *Tnf*$^{-/-}$ background, demonstrating the important role of TNF-independent death in this model. Tamoxifen delivery by intraperitoneal (*i.p.*) oil injection has been reported to cause peritoneal inflammation, foam cell formation, and depletion of resident macrophages (51). To exclude the possibility that sterile peritonitis contributes to TNF-independent death in *A20/Abin-1*$^{T-\Delta IEC}$*Tnf*$^{-/-}$ mice, we treated mice with tamoxifen by oral gavage rather than *i.p*. A higher dose of tamoxifen was required to delete A20 and ABIN-1 in IECs from the small intestine and colon by oral gavage (**Supplemental Figure 1A**), and with this approach *A20/Abin-1*$^{T-\Delta IEC}$*Tnf*$^{-/-}$ mice died with similar kinetics as *A20/Abin-1*$^{T-\Delta IEC}$ mice (**Figure 1A**). Enteroids derived from *A20/Abin-1*$^{T-\Delta IEC}$*Tnf*$^{-/-}$ mice undergo deletion of A20 and ABIN-1 when treated with 200nM 4-hydroxytamoxifen (4-OHT) *in vitro,* but they are protected from spontaneous cell death (**Supplemental Figure 1B-D**). This suggests that IEC-extrinsic factors *in vivo* drive TNF-independent IEC death and mortality in *A20/Abin-1*$^{T-\Delta IEC}$*Tnf*$^{-/-}$ mice. Since *in vitro* IEC enteroid cultures are sterile, we considered that microbial signals might promote death *in vivo*. While our prior studies suggested that broad spectrum antibiotic treatment was insufficient to rescue *A20/Abin-1*$^{T-\Delta IEC}$*Tnf*$^{-/-}$ mice (9), we hypothesized that residual microbes in these mice could trigger IEC death in these mice. Accordingly, we derived *A20/Abin-1*$^{T-\Delta IEC}$*Tnf*$^{-/-}$ germ-free mice by cesarean section. *Tnf*$^{-/-}$ germ-free mice were largely protected from death upon deletion of *A20* and *Abin-1* in IECs (**Figure 1B**). To control for developmental alterations by germ-free derivation, we conventionalized germ-free *A20/Abin-1*$^{T-\Delta IEC}$*Tnf*$^{-/-}$ mice with cecal contents from corresponding specific-pathogen free (SPF) mice in our facility. Germ-free mice

4

conventionalized with cecal contents from SPF $A20/Abin-1^{T-\Delta IEC}Tnf^{-/-}$ mice (GF-CONV) exhibited rapid mortality upon deletion of $A20$ and $Abin-1$ (**Figure 1B**), suggesting the increased survival of germ-free mice was not due to a developmental aberration. Therefore, microbial signals contribute to TNF-independent IEC death in the setting of acute $A20$ and $Abin-1$ deletion.

Although germ-free $A20/Abin-1^{T-\Delta IEC}Tnf^{-/-}$ mice exhibited increased survival, it was unclear whether this was due to reduced IEC death or merely due to broadly reduced septic sequelae under germ-free conditions. Histologically, acute deletion of $A20$ and $Abin-1$ in the intestinal epithelium caused rapid intestinal epithelial denudation, inflammatory infiltrate, cryptitis, and loss of mucosal architecture in both the small intestine and colon within 40 hours in SPF conventionalized mice (**Figure 1C,D**). In contrast, germ-free $A20/Abin-1^{T-\Delta IEC}Tnf^{-/-}$ mice exhibited far less histologic injury (**Figure 1C,D**). Since IEC loss in this model is further characterized by massive apoptotic IEC death, we performed cleaved caspase 3 (CC3) immunohistochemistry. In parallel to the reduction in histologic disease severity, we observed dramatically reduced CC3 in IECs of germ-free $A20/Abin-1^{T-\Delta IEC}Tnf^{-/-}$ mice as compared to SPF conventionalized counterparts (**Figure 1E,F**).

These results highlight that $A20/Abin-1^{T-\Delta IEC}Tnf^{-/-}$ mice provide a window into studying TNF-independent IEC death. $A20/Abin-1^{T-\Delta IEC}Tnf^{-/-}$ mice die due to spontaneous fulminant IEC death *in vivo*, but those IECs survive *in vitro* in the absence of hematopoietic cells, autocrine TNF, and microbial stimuli. When microbial stimuli are removed under germ-free conditions, the $A20$ and $Abin-1$-deficient IECs survive *in vivo* even with hematopoietic cells and other potential cytotoxic factors present. Interestingly, some germ-free $A20/Abin-1^{T-\Delta IEC}Tnf^{-/-}$ mice die (**Figure 1B**), suggesting that there may be some sterile inflammatory factors that can contribute to TNF-independent IEC death, but microbial factors are a primary driver of intestinal inflammation in this model.

Deletion of *MyD88*, and to a lesser extent *Trif*, rescues $A20/Abin-1^{T-\Delta IEC}Tnf^{-/-}$ mice

Given the dramatic improvement in survival and intestinal epithelial integrity in germ-free $A20/Abin-1^{T-\Delta IEC}Tnf^{-/-}$ mice, we hypothesized that microbial signaling through $MyD88$ mediated intestinal inflammation in this model. To facilitate combining of multiple mutant alleles, we targeted $MyD88$ in $A20/Abin-1^{T-\Delta IEC}Tnf^{-/-}$ zygotes as

5

previously described (52). Using two guides targeting exon 1 of *MyD88,* we generated two founder strains of mice with deletions at the *MyD88* locus, *A20/Abin-1$^{T-\Delta IEC}$Tnf$^{-/-}$MyD88$^{-/-}$ C1* and *C2* (**Figure 2A, Supplemental Figure 2A,B**). We confirmed deletion of MYD88 at the protein level in both mouse strains (**Figure 2B**). *A20/Abin-1$^{T-\Delta IEC}$Tnf$^{-/-}$MyD88$^{-/-}$ C1* and *C2* behaved identically, and so are presented in aggregate for clarity. Heterozygous deletion of *MyD88* conferred a modest improvement in survival, while complete deletion of *MyD88* led to a marked improvement in survival in *A20/Abin-1$^{T-\Delta IEC}$Tnf$^{-/-}$* mice (**Figure 2C**). The histologic phenotype paralleled the survival benefit, where the intestinal epithelium from *A20/Abin-1$^{T-\Delta IEC}$Tnf$^{-/-}$MyD88$^{-/-}$* mice exhibited significantly less inflammatory injury in the small intestine and colon as compared *A20/Abin-1$^{T-\Delta IEC}$Tnf$^{-/-}$* mice (**Figure 2D,E**). Similarly, deletion of *MyD88* significantly reduced the frequency of apoptotic CC3+ IECs as compared to their *MyD88$^{+/+}$* counterparts (**Figure 2F,G**). *A20/Abin-1$^{T-\Delta IEC}$Tnf$^{-/-}$MyD88$^{+/-}$* mice exhibited intermediate histologic injury and CC3 frequency **(Figure 2D-G)**. These results are surprising given that *MyD88* plays a critical role in intestinal homeostasis, and deletion has been reported increase susceptibility to other mouse models of colitis (53–55).

MyD88 expression in IECs maintains intestinal epithelial integrity and homeostasis (54, 55). Given the improved survival of *A20/Abin-1$^{T-\Delta IEC}$Tnf$^{-/-}$MyD88$^{-/-}$* mice, we next examined whether MYD88 activation directly induces apoptotic IEC death using *A20/Abin-1$^{T-\Delta IEC}$Tnf$^{-/-}$* primary small intestinal enteroid cultures. MYD88 mediates signaling downstream of both Toll-like receptors (TLRs) and IL-1 family members (56, 57), so we stimulated IECs with pam3CSK4 (a TLR2/1 agonist). This ligand did not induce significant death in *A20/Abin-1$^{T-\Delta IEC}$Tnf$^{-/-}$* enteroids (**Figure 3A**). Similarly, IL-1β and IL-18, two IL-1 family members that activate MYD88, did not directly induce death in *A20/Abin-1$^{T-\Delta IEC}$Tnf$^{-/-}$* enteroids (**Figure 3A, Supplemental Figure 3A**). Although *MyD88* deletion rescues *A20/Abin-1$^{T-\Delta IEC}$Tnf$^{-/-}$* mice, MYD88 activation was not sufficient for IEC death *in vitro*.

TRIF contains a RIP homotypic interaction motif (RHIM) domain and interacts with RIPK3 to induce death signaling downstream of TLR3 in response to the dsRNA analog polyinosinic-polycytidylic acid (poly(I:C)) (44, 58–61). We tested the susceptibility of *A20/Abin-1$^{T-\Delta IEC}$Tnf$^{-/-}$* enteroids to poly(I:C)-induced death, and we observed that deletion of *A20* and *Abin-1* in IECs dramatically increased susceptibility to poly(I:C)-induced

death (**Figure 3A**). LPS, in contrast, induced minimal cytotoxicity (**Figure 3A**). Both poly(I:C) and LPS activate TRIF, but IEC-death in response to LPS has previously been reported to depend on TNF, in contrast to poly(I:C) (44). We deleted *Trif* in *A20/Abin-1*$^{T-ΔIEC}$*Tnf*$^{-/-}$ mice using CRISPR/Cas9 editing and generated a strain of mice with a deletion and premature stop codon at the *Trif* locus (**Supplemental Figure 3B,C**). Splenocytes derived from *A20/Abin-1*$^{T-ΔIEC}$*Tnf*$^{-/-}$*Trif*$^{-/-}$ mice exhibited significantly reduced IFN-β production in response to poly(I:C), confirming functional deletion at the protein level (**Supplemental Figure 3D**). To determine if *Trif* deletion protected *A20* and *Abin-1* deficient IECs from TNF-independent death *in vitro*, we expanded enteroid cultures from these mice. *A20/Abin-1*$^{T-ΔIEC}$*Tnf*$^{-/}$*Trif*$^{-/-}$ enteroids were almost entirely resistant to poly(I:C) and LPS-induced cell death (**Figure 3A**). Therefore, A20 and ABIN-1 cooperatively restrict TRIF-mediated death in response to TLR3 and TLR4 agonists *in vitro*.

Given that *Trif* deletion rescued TNF-independent death in response to poly(I:C) and LPS *in vitro*, we treated *A20/Abin-1*$^{T-ΔIEC}$*Tnf*$^{-/-}$*Trif*$^{-/-}$ mice with tamoxifen to see if *Trif* deletion also protected *A20* and *Abin-1* deficient IECs *in vivo*. Deletion of *Trif* in *A20/Abin-1*$^{T-ΔIEC}$*Tnf*$^{-/-}$ mice provided a modest survival benefit, with slightly delayed median survival relative to *Trif*$^{+/+}$ controls (**Figure 3B**). Interestingly, heterozygous and homozygous deletion of *Trif* conferred similar survival benefit. We examined the small intestine and colon at 40h after tamoxifen-induced deletion of *A20* and *Abin-1* in *A20/Abin-1*$^{T-ΔIEC}$*Tnf*$^{-/-}$*Trif*$^{-/-}$ mice and saw a trend toward improvement in histologic severity, but this was not statistically significant when compared to the *A20/Abin-1*$^{T-ΔIEC}$*Tnf*$^{-/-}$ mice (**Figure 3C,D**). Deletion of *Trif* did partially reduce CC3 frequency to some extent, but not enough to prevent lethality in the *A20/Abin-1*$^{T-ΔIEC}$*Tnf*$^{-/-}$ mice (**Figure 3E,F**). While poly(I:C) potently induces *Trif*-dependent cytotoxicity in *A20* and *Abin-1*-deficient IECs *in vitro*, deletion of *Trif* does not protect against TNF-independent intestinal injury *in vivo*.

Combined deletion of *Ripk3* and *Casp8* completely protects *A20/Abin-1*$^{T-ΔIEC}$ IECs from death

Deletion of *Trif* did not reverse apoptotic IEC death in *A20/Abin-1*$^{T-ΔIEC}$*Tnf*$^{-/-}$ mice, but A20 is known to inhibit necroptosis as well as apoptosis (24, 62), and combined deletion of *A20* and *Abin-1* sensitizes IECs to both Casp8-dependent apoptotic death and RIPK3-dependent necroptotic death *in vitro* (9). Deletion of *Ripk3* does not prevent IEC injury after acute deletion of *A20* and *Abin-1*, so we hypothesized that combined deletion of

Ripk3 and *Casp8* would rescue *A20/Abin-1$^{T-ΔIEC}$* mice. We performed CRISPR/Cas9 editing of the *Casp8* locus in *A20/Abin-1$^{T-ΔIEC}$Ripk3$^{-/-}$* mice. This yielded a strain of mice with a premature stop codon in exon 2 of *Casp8* (**Supplemental Figure 4A**), with deletion of CASP8 at the protein level confirmed by immunoblot (**Supplemental Figure 4B**). *A20/Abin-1$^{T-ΔIEC}$Ripk3$^{-/-}$* mice exhibited 100% lethality, but *A20/Abin-1$^{T-ΔIEC}$Ripk3$^{-/-}$Casp8$^{-/-}$* mice were completely protected from death after treatment with tamoxifen (**Figure 4A**). Histologically, *A20/Abin-1$^{T-ΔIEC}$Ripk3$^{-/-}$Casp8$^{-/-}$* mice exhibited markedly improved histologic disease severity (**Figure 4B,C**) and CC3 frequency was reduced to near background levels (**Figure 4D,E**). *In vitro*, enteroids derived from *A20/Abin-1$^{T-ΔIEC}$Ripk3$^{-/-}$Casp8$^{-/-}$* mice were completely protected from both spontaneous IEC death (**Figure 4F**) and TRIF-mediated cell death (**Supplemental Figure 4C**). These data collectively demonstrate that simultaneous suppression of both Casp8-dependent apoptosis and RIPK3-dependent necroptosis completely preserves IEC survival after acute deletion of *A20* and *Abin-1 in vitro* and *in vivo*.

LTα$_3$ induces apoptosis and necroptosis downstream of TNFR1 in *A20/Abin-1$^{T-ΔIEC}$Tnf$^{-/-}$* enteroids

As combined deletion of *Ripk3* and *Casp8* completely prevented IEC death after deletion of *A20* and *Abin-1*, but *Trif* deletion did not provide equivalent survival benefit, we hypothesized that another TNF superfamily member may be contributing to TNF-independent, IEC-extrinsic death *in vivo.* We previously reported that the TNF superfamily members TNF-like weak inducer of apoptosis (TWEAK), Fas ligand, and TNF-related apoptosis inducing ligand (TRAIL) failed to induce significant death of *A20/Abin-1$^{T-ΔIEC}$Tnf$^{-/-}$* enteroids *in vitro* (9). Here we tested receptor activator of nuclear factor kappa-B ligand (RANKL), "homologous to lymphotoxin, exhibits inducible expression and competes with HSV glycoprotein D for binding to herpesvirus entry mediator, a receptor expressed on T lymphocytes" (LIGHT), and TNF-like cytokine 1A (TL1A), none of which induced significant IEC death (**Figure 5A**).

Although none of those alternative TNF superfamily ligands induced death in *A20/Abin-1$^{T-ΔIEC}$Tnf$^{-/-}$* enteroids, we previously showed that deletion of *A20* and *Abin-1* increases sensitivity of the TNF receptor 1 (TNFR1) to TNF by 1000-fold in IECs (9). Given that TNFR1 sensitivity is significantly increased in *A20* and *Abin-1-* deficient IECs, we considered alternative TNFR1 ligands. Lymphotoxin alpha homotrimers (LTα$_3$) are reported to bind to TNFR1 and activate death signaling (63–65). We tested human LTα$_3$ and observed significant

8

increased susceptibility to death in *A20* and *Abin-1*-deficient IECs (**Figure 5B**). To test mouse $LT\alpha_3$, we generated a cell line constitutively expressing mouse $LT\alpha_3$-Fc fusion protein and validated the presence of soluble fusion protein (**Figure 5C**). $LT\alpha_3$-Fc fusion protein conditioned media ($LT\alpha_3$-Fc CM) induced significant death in *A20/Abin-1$^{T-\Delta IEC}$Tnf$^{-/-}$* enteroids (**Figure 5D**). Since $LT\alpha_3$-Fc CM could contain other factors that drive IEC death *in vitro*, we wanted to determine if a $LT\alpha$ monoclonal antibody reversed this activity *in vitro*. A $LT\alpha$-specific monoclonal antibody was previously developed and reported to inhibit collagen-induced arthritis (CIA) (66). We generated purified monoclonal antibody from this hybridoma and observed complete prevention of *A20/Abin-1$^{T-\Delta IEC}$Tnf$^{-/-}$* IEC death in response $LT\alpha_3$-Fc CM *in vitro* (**Figure 5E**). As a negative control, an isotype control antibody did not block cytotoxic activity (**Figure 5E**). Subsequently, we wanted to determine if TNF-independent IEC death in *A20* and *Abin-1*-deficient IECs in response to $LT\alpha_3$-Fc CM was indeed mediated by TNFR1. We added recombinant mouse $LT\alpha_1\beta_2$, which binds to LTBR but not TNFR1 (64), and we did not observe any cytotoxicity (**Figure 5F**). This argues that deletion of *A20* and *Abin-1* in IECs does not increase susceptibility to LTBR-mediated death. We added recombinant mouse LTBR-Fc and TNFR1-Fc fusion proteins and observed that only TNFR1-Fc completely protected *A20/Abin-1$^{T-\Delta IEC}$Tnf$^{-/-}$* enteroids from death (**Figure 5G**). These data demonstrate that deletion of *A20* and *Abin-1* in IECs unveils a profound sensitivity to $LT\alpha_3$-induced death downstream of TNFR1. It is important to highlight that the death assays we performed used primary, non-immortalized IECs in the absence of any death-sensitizing agents (e.g., cycloheximide), unlike most prior studies investigating TNF and $LT\alpha_3$-induced death (Chaturvedi et al., 1994; Etemadi et al., 2013).

Having determined that A20 and ABIN-1-deficient IECs are sensitized to $LT\alpha_3$-induced death downstream of TNFR1, we wanted to ascertain if $LT\alpha_3$-induced death was primarily apoptotic or necroptotic. Receptor interacting serine/threonine kinase 1 (RIPK1) binds caspase 8 and RIPK3, and RIPK1's kinase activity can support both apoptotic and necroptotic death (43, 45, 67, 68). Necrostatin-1s (Nec1s) is a small molecule RIPK1 kinase inhibitor that suppresses necroptosis and partially suppresses apoptosis (9, 69). As expected, the addition of Nec1s partially prevented $LT\alpha_3$-induced death in *A20/Abin-1$^{T-\Delta IEC}$Tnf$^{-/-}$* enteroids (**Figure 6A**). Caspase inhibition increases RIPK3-dependent necroptosis (70–72). Addition of emricasan, a pharmacologic pan-caspase inhibitor, caused increased death in response to $LT\alpha_3$, indicating that *A20/Abin-1$^{T-\Delta IEC}$Tnf$^{-/-}$* enteroids are sensitized to $LT\alpha_3$-induced necroptosis. In agreement with these *in vitro* death assays, deletion of

9

A20 and ABIN-1 in $A20/Abin\text{-}1^{T\text{-}\Delta IEC}Tnf^{-/-}$ enteroids leads to significantly increased CC3, cleaved caspase 8 (CC8), and cleaved PARP in response to $LT\alpha_3$ as compared to control $A20^{fl/fl}Abin\text{-}1^{fl/fl}Tnf^{-/-}$ enteroids (**Figure 6B**). There was no significant increase in phosphorylated RIPK3 (pRIPK3) (**Figure 6B**). This pattern is consistent with apoptosis as the primary mode of death in $A20/Abin\text{-}1^{T\text{-}\Delta IEC}Tnf^{-/-}$ enteroids in response to $LT\alpha_3$. The addition of Nec1s partially reduced CC3 and CC8 (**Figure 6B**), which is consistent with partial inhibition of apoptosis in response to RIPK1 kinase activity inhibition. The addition of emricasan reduced CC3 and CC8 but markedly increased pRIPK1 and pRIPK3, consistent with increased $LT\alpha_3$-induced necroptotic death when caspase activity is inhibited (**Figure 6B**). These data demonstrate that combined deletion of *A20* and *Abin-1* sensitizes IECs to both TNF-independent apoptosis and necroptosis in response to $LT\alpha_3$, although apoptosis is the dominant death pathway.

To further examine necroptosis and apoptosis, we stimulated enteroids derived from $A20/Abin\text{-}1^{T\text{-}\Delta IEC}Ripk3^{-/-}$ and $A20/Abin\text{-}1^{T\text{-}\Delta IEC}Ripk3^{-/-}Casp8^{-/-}$ mice with TNF and $LT\alpha_3$. The addition of exogenous TNF or $LT\alpha_3$ did not induce any additional cytotoxicity in $A20/Abin\text{-}1^{T\text{-}\Delta IEC}Ripk3^{-/-}Casp8^{-/-}$ enteroids (**Figure 6C**). These *in vitro* death assays demonstrate that simultaneous blockade of RIPK3-dependent necroptosis and CASP8-dependent apoptosis is required to rescue A20 and ABIN-1-deficient IECs from death in response to TNF or $LT\alpha_3$. We next examined death signaling in $A20/Abin\text{-}1^{T\text{-}\Delta IEC}Ripk3^{-/-}$ and $A20/Abin\text{-}1^{T\text{-}\Delta IEC}Ripk3^{-/-}Casp8^{-/-}$ enteroids. Consistent with our prior studies, $A20/Abin\text{-}1^{T\text{-}\Delta IEC}Ripk3^{-/-}$ enteroids demonstrated increased spontaneous CC3 and CC8 upon deletion of *A20* and *Abin-1*, as compared to $A20^{fl/fl}Abin\text{-}1^{fl/fl}$ enteroids (**Figure 6D**). $A20/Abin\text{-}1^{T\text{-}\Delta IEC}Ripk3^{-/-}Casp8^{-/-}$ enteroids, in contrast, did not exhibit CC3, CC8, or cleaved PARP relative to $A20^{fl/fl}Abin\text{-}1^{fl/fl}$ enteroids, even in the presence of exogenous $LT\alpha_3$ (**Figure 6D**). Therefore, combined deletion of RIPK3-dependent necroptosis and CASP8-dependent apoptosis completely protects $A20/Abin\text{-}1^{T\text{-}\Delta IEC}$ IECs from TNF- or $LT\alpha_3$-induced apoptotic and necroptotic death downstream of TNFR1.

LTα blockade combined with partial deletion of *MyD88* protects against TNF-independent death in $A20/Abin\text{-}1^{T\text{-}\Delta IEC}Tnf^{-/-}$ mice

To determine if $LT\alpha_3$ contributes to IEC injury *in vivo*, we first performed chromogenic RNA-*in situ* hybridization (RNA-ISH) for *Lta* in the intestine after IEC-deletion of *A20* and *Abin-1*. $A20/Abin\text{-}1^{T\text{-}\Delta IEC}Tnf^{-/-}$ mice exhibited

increased *Lta* positive cells in both the small intestine and colon as compared to $A20^{fl/fl}Abin\text{-}1^{fl/fl}Tnf^{-/-}$ mice, correlating increased *Lta* frequency with histologic severity upon deletion of *A20* and *Abin-1* in IECs (**Figure 7A,B**). Similarly, qPCR analysis of the small intestine and colon demonstrated increased *Lta* mRNA in $A20/Abin\text{-}1^{T\text{-}\Delta IEC}Tnf^{-/-}$ mice as compared to $A20^{fl/fl}Abin\text{-}1^{fl/fl}Tnf^{-/-}$, $A20/Abin\text{-}1^{T\text{-}\Delta IEC}Tnf^{-/-}MyD88^{-/-}$, and germ-free $A20/Abin\text{-}1^{T\text{-}\Delta IEC}Tnf^{-/-}$ mice (**Figure 7C**). The increased *Lta* mRNA by RNA-ISH and qPCR paralleled the pattern of intestinal injury we observed in mice with these genotypes.

To further understand if blocking LTα provided a survival benefit in these mice, we administered a monoclonal blocking antibody against LTα to $A20/Abin\text{-}1^{T\text{-}\Delta IEC}Tnf^{-/-}MyD88^{+/+}$ mice and observed a very small but statistically significant increase in weight and median survival as compared to isotype control, with survival increasing from 4.5 to 5.0 days (**Figure 7D,E**). As we observed a partial improvement in survival in our $A20/Abin\text{-}1^{T\text{-}\Delta IEC}Tnf^{-/-}MyD88^{+/-}$ mice, we administered anti-LTα to these mice and observed a statistically significant improvement in their weight curve, and an increase in median survival from 4.0 to 9.0 days (**Figure 7F,G**). Blocking LTα *in vivo* reduces weight loss and improves survival, particularly when combined with partial deletion of *MyD88*, supporting a model where both microbial signals and LTα contribute to TNF-independent intestinal injury in A20 and ABIN-1-deficient intestinal epithelium.

DISCUSSION

Genome-wide association studies have implicated hundreds of genes in CD and UC pathogenesis, but it is unclear how these genes increase disease susceptibility or influence treatment response (73). Since IBD is primarily a complex polygenic disease, except for rare monogenic causes, it follows that model systems often incorporate multiple genes simultaneously to decipher these complex epistatic genetic interactions. While we previously showed that A20 and ABIN-1 cooperatively restrict TNF-dependent IEC injury, this study demonstrates that A20 and ABIN-1 preserve intestinal homeostasis and IEC survival by restricting TNF-independent inflammatory injury. Microbial signals, MyD88 activation, and LTα all contribute to TNF-independent intestinal inflammation in the setting of acute A20 and ABIN-1 deletion in IECs. IEC death induced by A20 and ABIN-1 deficiency can also be blocked by simultaneous inhibition of CASP8-dependent apoptosis and RIPK3-dependent necroptosis. Given that A20 and ABIN-1 restrict both TNF-dependent and TNF-

11

independent IEC injury, this study further reveals why these proteins have such potent anti-inflammatory functions in the intestine. Although many previous studies focus on the role of A20 and ABIN-1 in hematopoietic cells, this study and others add to our understanding of the important role these proteins play in non-hematopoietic cells to preserve tissue integrity (9, 16, 38, 40).

Combined acute deletion of A20 and ABIN-1 in the intestinal epithelium is unique in both severity and TNF-independence when compared to deletion of other genes in IECs. For example, the fatal enteritis and colitis that develops after simultaneous deletion of A20 and ABIN-1 in IECs exceeds the severity reported for intestinal epithelial deletion of NEMO (45, 74), FADD (46, 75), CASP8 (46, 72), RIPK1 (43, 76), ATG16L1 (8), or combined deletion of XBP1 and ATG16L1 (7). Acute deletion of SETDB1 (77) in IECs induces mouse lethality with similar kinetics to the combined deletion of A20 and ABIN-1, although SETDB1$^{-/-}$ IECs die primarily from necroptotic cell death. The TNF-independent IEC death observed in *A20/Abin-1$^{T-ΔIEC}$Tnf$^{-/-}$* mice is also unusual when compared to other models. The colitis in mice with conditional IEC knock-out of NEMO, FADD, CASP8, and RIPK1 mice is largely reversed by TNF or TNFR1 deletion (43, 45, 46, 74–76). Similarly, the ileitis induced after knock-out of XBP1 in IECs is rescued by TNFR1 deficiency (7). Among these models, deletion of A20 and ABIN-1 is unique in that TNF deletion does not confer any significant survival benefit, and it does not appreciably reduce intestinal injury.

The ileal enteropathy associated with IEC knock-out of NEMO, FADD, or CASP8 is TNFR1-independent, even though colitis in those mice is TNFR1-dependent. Those models provide some perspective on the TNF-independent IEC death observed in *A20/Abin-1$^{T-ΔIEC}$Tnf$^{-/-}$* mice. Paneth cell loss after IEC knock-out of FADD and CASP8 is partially reduced by TNFR1 deletion but is further reduced by deletion of Z-DNA binding protein 1 (ZBP1), suggesting that ZBP1 contributes to TNFR1-independent death in the ileum (46).
ZBP1 is an interferon-inducible gene product that interacts with RIPK3 via its RHIM domain and activates necroptotic cell death in response to type I & II interferons (78) and viral nucleic acids (79). It is possible that ZBP1 contributes to TNF-independent IEC death after deletion of A20 and ABIN-1, especially since deletion of TRIF only modestly increased median survival. However, ZBP1 has been shown to activate RIPK3 in IECs when FADD-CASP8-apoptotic death is inhibited (46), or in response to RNA from reactivated endogenous

12

retroviruses after SETDB1 deletion (77). In *A20/Abin-1$^{T-\Delta IEC}$Tnf$^{-/-}$* IECs, both FADD and CASP8 are present to activate apoptotic death, and CC3 is detected in the intestinal epithelium and in intestinal organoids, favoring a central role for CASP8-dependent apoptosis rather than potential ZBP1-dependent necroptosis as the dominant TNF-independent death pathway. In *A20/Abin-1$^{T-\Delta IEC}$Tnf$^{-/-}$* IECs, RIPK1 is also present and would be predicted to inhibit ZBP1-mediated activation of RIPK3 (80). We cannot entirely exclude a role for ZBP1 in TNF-independent IEC death after deletion of A20 and ABIN-1, but the dominant death pathway in *A20/Abin-1$^{T-\Delta IEC}$Tnf$^{-/-}$* mice is most consistent with CASP8-mediated apoptosis.

Gasdermin D (GSDMD)-mediated pyroptotic death is another potential TNF-independent death pathway to consider in A20 and ABIN-1 deficient IECs. A20 restricts NLRP3 inflammasome activation (35, 81), so increased susceptibility to pyroptotic death is a possible sequela of acute simultaneous A20 and ABIN-1 deletion in IECs. Canonical inflammasome activation culminates in cleaved caspase-1 and non-canonical inflammasome activation culminates in cleaved caspase-11 in mice (82). Both cleaved caspase-1 and -11 can cleave GSDMD, which in turn causes pyroptotic death (83, 84). Caspase-1 or -11 cleavage of GSDMD could theoretically precipitate pyroptotic death in *A20/Abin-1$^{T-\Delta IEC}$Tnf$^{-/-}$* mice. Combined deletion of RIPK3 and CASP8 completely rescues A20 and ABIN-1-deficient IECs from death, even when caspase-1 and-11 are present, but RIPK3 regulates inflammasome activation independent of its role in necroptotic death (35, 85, 86), and CASP8 has been reported to mediate GSDMD cleavage under certain conditions (87, 88). This raises the possibility that combined deletion of RIPK3 and CASP8 rescues *A20/Abin-1$^{T-\Delta IEC}$* mice due to simultaneous blockade of apoptotic, necroptotic, and pyroptotic death. However, GSDMD-dependent death has been reported in IECs primarily when either FADD-deficiency or catalytically inactive Casp8 are combined with MLKL deficiency (46, 89, 90). Those recent studies suggest that IECs are driven more toward pyroptotic death when apoptosis and necroptosis are inhibited. A central role for pyroptosis therefore would be less likely in *A20/Abin-1$^{T-\Delta IEC}$Tnf$^{-/-}$* mice, where FADD, active CASP8, RIPK1, RIPK3, and MLKL are all present. Taken together, it is possible that some amount of GSDMD-mediated pyroptotic damage occurs in parallel to apoptotic and necroptotic IEC death in *A20/Abin-1$^{T-\Delta IEC}$Tnf$^{-/-}$* mice, but apoptotic death is the primary death pathway.

There are multiple potential translational implications for the findings that $LT\alpha_3$ and MYD88 contribute to TNF-independent intestinal damage in this model of severe enterocolitis. Deletion of A20 and ABIN-1 unveils a role for $LT\alpha_3$-induced TNF-independent IEC death in primary cells both *in vivo* and *in vitro*. To our knowledge, this is the first description of TNF-independent $LT\alpha_3$-induced cytotoxicity in IECs in the absence of death-sensitizing agents. There are many potential mechanisms by which patients with IBD may fail to respond to anti-TNF therapy, including activation of alternative inflammatory pathways, neutralizing antibodies, subtherapeutic levels, or inability to block autocrine IEC-derived TNF, but it is tempting to consider whether $LT\alpha_3$-mediated TNFR1-induced IEC death could play a role in a subset of patients. Polymorphisms in *LTA* were associated with anti-TNF non-response in a small cohort of patients (14), but this was not reproduced in a larger cohort (91). Moreover, Etanercept, a soluble TNFR2-Fc receptor which blocks TNF and $LT\alpha_3$ was ineffective for CD (92). On the other hand, subsequent data suggests that Etanercept is ineffective in part because it does not induce antibody-dependent cell-mediated cytotoxicity or apoptosis of pathogenic TNF-expressing inflammatory cells to the same extent as anti-TNF antibodies (93, 94). Intriguingly, the combination of an anti-TNF monoclonal antibody to neutralize TNF plus Etanercept which additionally neutralizes $LT\alpha_3$ was effective in a case report of a patient with severe HLA-B27-associated arthropathy who had failed treatment with either agent alone (95). The other TNF-independent injury pathway highlighted in this study is MYD88. Microbial signals activating MYD88 in the hematopoietic compartment contribute to intestinal injury, but it would be instructive to understand which microbes are most pathogenic in *A20/Abin-1$^{T-\Delta IEC}$Tnf$^{-/-}$* gnotobiotic mice. Interestingly, the fact that some germ-free *A20/Abin-1$^{T-\Delta IEC}$Tnf$^{-/-}$* mice die suggests that sterile inflammation is sufficient to induce death. MYD88 mediates signaling downstream of IL-1β and IL-18 which could potentially explain the death of some germ-free *A20/Abin-1$^{T-\Delta IEC}$Tnf$^{-/-}$* mice. Both IL-1β and IL-18 have been proposed as potential mediators of anti-TNF non-response in patients with IBD (96–98). Ultimately, having animal models to investigate TNF-independent intestinal injury could prove useful in understanding anti-TNF non-response in subsets of patients.

In summary, we discovered that microbial signals, MYD88 signaling, and $LT\alpha_3$ drive severe TNF-independent enterocolitis after acute deletion of two IBD-associated genes *A20* and *Abin-1*, which can be prevented by combined deletion of *Ripk3* and *Casp8.* This study highlights that A20 and ABIN-1 cooperatively maintain

14

intestinal homeostasis by inhibiting both TNF-dependent and TNF-independent inflammatory intestinal injury. Understanding the genetic determinants of intestinal epithelial health, their epistatic relationships, and how they could influence therapeutic response in models of IBD will provide important mechanistic insights to inform future translational studies.

Methods

Mice

$A20^{fl}$ and $Abin-1^{fl}$ mice were generated in the Ma laboratory and were described previously (9, 28, 62, 99). $Tnf^{-/-}$ mice were purchased from Jackson Laboratories (Bar Harbor, MA), X. Wang provided $Ripk3^{-/-}$ mice, and transgenic mice with a tamoxifen-inducible Cre recombinase under the control of the villin-promoter ($Vil-cre-ER^{T2+}$) mice were a kind gift from S. Robine (Institut Curie-CNRS, Paris, France) (100). These alleles were backcrossed to $A20^{fl}$ and $Abin-1^{fl}$ mice transgenic mice for > 8 generations as previously described (9). Acute deletion of floxed $A20$ and $Abin-1$ exons $in vivo$ by oral gavage was performed using tamoxifen (2 mg/day, Sigma, T5648) for 3 consecutive days as indicated for survival analysis. $MyD88^{+/-}$ and $Trif^{+/-}$ breeders were maintained on antibiotic water $ad libitum$ with ampicillin 1mg/ml (Sigma), vancomycin 0.5mg/ml (Sigma), and neomycin 1mg/ml (Sigma), and offspring were transitioned to regular water at weaning. For $in vivo$ monoclonal antibody treatment, mice were injected with 370μg of antibody on days -2, 0, 1, 2, 5, 7, and 9. For all experimental mice, genotypes were confirmed twice. When possible, littermates were used as controls. Both males and females were included in all experiments with no observable gender differences. Mice were analyzed between 7-12 weeks of age for all experiments.

Germ-free derivation, maintenance, and conventionalization

Germ-free A20/Abin-1$^{T-ΔIEC}Tnf^{-/-}$ mice were derived by Cesarean delivery into the UCSF Gnotobiotic Core Facility (gnotobiotics.ucsf.edu) and maintained in germ-free isolators. Stool pellets from isolators in the Gnotobiotic facility were screened every 2-3 weeks by culture and qPCR, whenever mice were transferred from breeding to experimental isolators, and at the beginning and end of each experiment. 515F and 806R universal primers were used to amplify the V4 region: 515F-GTGCCAGCMGCCGCGGTAA; 806R-GGACTACHVGGGTWTCTAAT. For cecal content conventionalization experiments, cecal contents from specific-pathogen free (SPF) mice were resuspended in 10% weight/volume (w/v) Bacto Brain Heart Infusion

15

(BHI) (VWR) supplemented with 0.05% w/v L-cysteine (Sigma) in aerobic conditions, filtered over a 100μm filter, and 200μl was administered to germ-free mice by oral gavage 5-7 days prior to tamoxifen treatment.

CRISPR/Cas9 editing of *MyD88*, *Trif*, and *Casp8*

Two guide RNAs for each target gene were designed using Benchling (Benchling, San Francisco, CA). The following guide RNAs (gRNAs) were selected for editing A20/Abin-1$^{T\text{-}\Delta IEC}$*Tnf*$^{-/-}$ mice: *MyD88* guide 1 CCCACGTTAAGCGCGACCAA and *MyD88* guide 2 AAGGAGCTGAAGTCGCGCAT targeting exon 1 of *MyD88*; *TRIF* guide 1 TCTGGAACGCTAATTTCGTG and *TRIF* guide 2 CAAGCTATGTAACACACCGC targeting exon 2 of *Trif*. The following gRNAs were selected for editing A20/Abin-1$^{T\text{-}\Delta IEC}$*Ripk3*$^{-/-}$ mice: *Casp8* guide 1 TAGCTTCTGGGCATCCTCGA and *Casp8* guide 2 CTTCCTAGACTGCAACCGAG targeting exon 2 of *Casp8*. The corresponding crRNAs targeting each gene and tracrRNA were annealed and ribonucleoprotein (RNP) complexes were prepared with HiFi Cas9 nuclease ribonucleoprotein (IDT) according to manufacturer instructions. RNPs were electroporated into mouse zygotes as previously described (52), with the main exception that the standard square curve electroporation (two pulses at 30V for 3 ms with an interval of 100 ms) was performed once or four times with an interval of 3s Gene Pulser Xcell (Biorad). Zygotes were cultured to two-cell embryos and transferred into pseudopregnant females. All mutations were confirmed by cloning and sequencing. Mice with a confirmed deletion or premature stop codon were then backcrossed 3 generations to the parental strains to breed out off-target edits before analysis.

Intestinal Epithelial Cell Enteroid Culture and Confocal Microscopy

For enteroid culture, intestinal crypts were isolated from the small intestine as previously described(101), with the modifications of substituting 10% R-spondin-1 conditioned medium for recombinant R-spondin1, and the addition of Normocin (100 mg/ml, Invivogen). R-spondin1 expressing 293T cells were a kind gift from Dr. Noah Shroyer (Baylor College of Medicine). For all enteroid experiments, enteroids were derived from at least 2 mice on separate occasions and representative data are shown. Deletion of *A20* or *Abin-1 in vitro* was performed via treatment with 4-OHT (200nM, Sigma). Confocal imaging of enteroids was performed on a Leica SP5 laser scanning confocal system (Leica Microsystems) using a 10X dry objective. Images were acquired in a format of 512x512, with a line average of at least 3, scan speed of 400 Hz, and pinhole airy unit 1. Excitation for both PI and brightfield was done with the 488nm laser line at 30% power with a detection band of 550-732nm. Image analysis was performed on the Leica Application Suite (Leica Microsystems).

16

Cell Death Assays

Enteroid death assays were performed by resuspending in Matrigel (Corning) and plating 25µl per well in 96-well flat-bottom opaque plates (Nunc). After 24h, enteroids were stimulated as indicated to a final volume of 200µl. Viability was measured using the CellTiter Glo 3D assay (Promega) according to the manufacturer's specifications, with the exception that 100µl of reagent was added to 200µl of culture for a final volume of 300µl prior to reading. Luminescence was read on a SpectraMax M5® (Molecular Devices), analyzed using SoftMax Pro (Molecular Devices), and expressed as percent viability relative to vehicle control.

Cell Signaling Assays and Immunoblot Analysis

For enteroid lysates, cultures were resuspended in Cell Recovery Solution (Corning) supplemented with 10µM Y-27632 (Calbiochem) and incubated for 15min on ice, followed by centrifugation at 500xg for 5min. Cell pellets were lysed in ice-cold NP40 lysis buffer (1% NP40 v/v, 50mM Tris HCl pH 7.4, 150mM NaCl, and 10% glycerol v/v) supplemented with complete EDTA-Free Protease Inhibitor Cocktail (Roche), phosphatase inhibitors (1mM Na3VO4 and 10mM NaF), and 10mM N-ethylmaleimide. After lysis, samples were centrifuged for 20min at 21,130xg to remove debris, and the supernatants were quantitated using the BCA Protein Assay Kit (Pierce). Lysates were normalized and denatured in LDS Sample Buffer (Invitrogen), followed by resolution on NuPage precast 4-12% Bis-Tris gels (Invitrogen) and transferred to PVDF for immunoblotting.

qPCR

1cm of small intestine or colon was flushed with saline solution and placed in RNAlater (ThermoFisher Scientific) and stored at 4C. The following day, the solution was aspirated, and samples were stored at -70C. Samples were then thawed and homogenized in Buffer RLT (Qiagen) supplemented with β-mercaptoethanol using Lysing Matrix D tubes (MP Biomedicals) on the FastPrep-24 (MP Biomedicals), followed by QIAshredder homogenization (Qiagen). RNA was prepared using the RNeasy Mini Kit (Qiagen) with on-column DNase digestion according to manufacturer's instructions. Quality was confirmed using the NanoDrop ND-1000 (ThermoFisher Scientific) and Agilent RNA 6000 Nano Kit on the Agilent 2100 Bioanalyzer (Agilent), according to manufacturer's instructions. cDNA was synthesized from 2000ng of total RNA using the High-Capacity RNA-to-cDNA kit (Thermo Scientific). qPCR was performed using TaqMan probes for mouse *Lta* (Mm00440228_gH) and mouse *Actb* (Mm02619580_g1), and the TaqMan® Universal Master Mix II with UNG on the QuantStudio 6 (ThermoFisher Scientific). Relative gene abundance was normalized to the mean expression of the house-

keeping gene *Actb*, and $2^{-\Delta\Delta Ct}$ was calculated relative to *A20^fl/fl^Abin-1^fl/fl^Tnf^−/−^*. All samples were run in duplicate. Data were analyzed using QuantStudio RealTime PCR Software (Thermo Scientific).

Histology and Immunohistochemistry

Mice were individually euthanized, dissected, and their resected intestinal tissue was immediately fixed in 10% neutral-buffered formalin (Sigma) 40h after treatment with tamoxifen. Tissue specimens were fixed for 16-24 hours, washed in PBS three times, then placed in 70% ethanol and shipped to Histowiz (Brooklyn, NY) for paraffin embedding, sectioning, staining, and high-resolution (40X) scanning according to standard protocols. H&E histologic severity quantitation was performed using a scoring system previously described for genetic IBD models affecting the small intestine (score range 0-15) or colon (score range 0-12) (102). For CC3-stained sections (Cell Signaling Technology 9661), 10 consecutive crypts from each of 5 sections for small intestine and colon (50 crypts per mouse per segment) were counted. Chromogenic RNA *in situ hybridization* (RNA-ISH) was performed using RNAscope® Probe- Mm-*Lta* (Advanced Cell Diagnostics 317231) and RNAscope 2.5 HD Assay- Brown Kit (Advanced Cell Diagnostics 322370) according to the manufacturer's specifications. Slides were immediately covered with a coverslip using Cytoseal. Slides were then scanned at 40X magnification with a Zeiss Axio ScanZ.1 (Zeiss). DAB-positive areas were identified against a hematoxylin background in all 5 sections of small intestine and colon on each slide using QuPath v0.2.3. At least two and up to three blinded readers assessed histologic disease severity, CC3 quantitation, and *Lta* quantitation and the results were averaged.

Antibodies and reagents

Antibodies directed against A20 (Cell Signaling Technology, 5630), ABIN-1 (Sigma HPA037893), Caspase 8 (Cell Signaling Technology mouse specific 4927 and 4790), CC8 (Cell Signaling Technology 8592), RIPK1 (Cell Signaling Technology 3493), Caspase 3 (Cell Signaling Technology 9662), CC3 (Cell Signaling Technology 9661), PARP (Cell Signaling Technology 9542), mouse RIPK3 (Cell Signaling Technology 95702), phospho-RIPK3 (T231/S232) (Cell Signaling Technology 91702), phospho-RIPK1 (Ser166) rodent specific (Cell Signaling Technology 31122), and GAPDH (Millipore MAB374), were used for western blot. Anti-CC3 (Cell Signaling Technology 9661) was also used for IHC studies. Mouse IFN-β ELISA (PBL assay bioscience) was used according to the manufacturer's instructions. Recombinant mouse TNF, mouse IL-18, mouse TL1A, mouse LT$\alpha_1\beta_2$, human LTα_3, mouse TNFR1-Fc, and mouse LTBR-Fc were purchased from R&D systems.

Recombinant mouse RANKL was purchased from BioLegend. Recombinant mouse IL-1β and mouse LIGHT were purchased from Peprotech. Pam3CSK4, poly(I:C) HMW, and LPS from E. coli O111:B4 were purchased from Invivogen. Necrostatin-1s (BioVision 2263) and Emricasan (MedChem Express HY-10396) were used at 50μM final concentration. S5H3.2.2 hybridoma cell line (ATCC) expressing monoclonal hamster anti-mouse LTα (66) was provided to BioXcell (Lebanon, New Hampshire) for production of purified monoclonal antibody for *in vivo* use. *InVivo*MAb Armenian hamster IgG isotype control anti-glutathione S-transferase (BioXcell #BE0260) was used as a negative control.

LTα_3-Fc conditioned media

Codon-optimized gblocks (IDT) encoding mouse LTα (amino acids 1-202; UniProtKB/Swiss-Prot P09225.1) followed by a GSG linker and mouse IgG2a Fc fusion (amino acid 99-330; UniProtKB/Swiss-Prot P01863) were synthesized and then cloned into pENTR (Addgene Plasmid #17398) using InFusion cloning according to manufacturer's instructions (Clontech). The insert sequence was confirmed and then cloned into pLEX_307 (Addgene Plasmid #41392) using the Gateway Cloning LR reaction according to manufacturer's instructions (ThermoFisher Scientific). Lentivirus particles were prepared by co-transfection with the packaging plasmid psPAX2 (Addgene Plasmid #12260) and the envelope plasmid pMD2.G (Addgene Plasmid #12259) into HEK293T (ATCC) cells using Lipofectamine 2000 (ThermoFisher Scientific). The lentivirus-containing medium was collected at 72 h post-transfection. After centrifugation, the lentivirus medium was filtered using a 0.45 µm syringe filter. HEK293T cells were transduced with diluted lentivirus and selected with puromycin 5 ug/ml for several passages. The puromycin was removed and mLTα-Fc conditioned media (mLTα-Fc CM) was collected and filtered over 0.22μm filter. The mLTα-Fc CM was quantitated by ELISA with goat polyclonal LTα capture antibody (R&D systems AF749), rat monoclonal LTα detection antibody (R&D systems MAB749) biotinylated with ChromaLink biotin according to manufacturer's instructions (Trilink Biotechnologies), a recombinant mouse lymphotoxin alpha ELISA reference (a gift from R&D systems), peroxidase streptavidin (Jackson ImmunoResearch), and 1-Step Ultra TMB-ELISA (ThermoFisher Scientific).

Statistics

Statistical analysis was performed with Graphpad Prism 9 (Graphpad Software, San Diego, CA). Kaplan-Meier survival curve comparisons were performed using the log-rank Mantel-Cox test. Comparisons between two groups were performed by two-tailed unpaired Student's t-test. Multigroup comparisons were performed by

one-way analysis of variance (ANOVA) if we were comparing one variable per group or two-way ANOVA if there were multiple variables per group. When comparing every mean to every other mean by ANOVA, Tukey's multiple comparison test was used. When comparing each mean to a control, Dunnett's multiple comparison test was used. When comparing only a subset of means, Bonferroni's multiple comparison test was used. $p < 0.05$ was used as the threshold for statistical significance. All experiments shown represent at least two independent repetitions.

Study approval

All animal studies were conducted in accordance with the University of California, San Francisco Institutional Animal Care and Use Committee (AN183350).

Author Contributions

M.G.K. and A. Ma conceived of the project. M.G.K. oversaw the project and designed and performed the experiments with assistance from I.R and E.M. I.R. performed *in vivo* experiments, *in vitro* death assays, and helped generate LTα_3-Fc CM. Co-first author order determined by duration of time spent on the project. E.M. performed enteroid immunoblot analysis and *in vitro* assays. E.M. and I.R. performed RNA-ISH analysis with advice and guidance from O.D.K. Z.L. performed CRISPR/Cas9 zygote editing with guidance from A. Marson. J.L.B., X.S., Y.Y.R, Z.W., R.A., and P.A. assisted with mouse breeding, genotyping, and histology quantitation. K.L., P.J.T., and J.A.T. derived germ-free mice and performed germ-free experiments in the UCSF Gnotobiotics Core Facility. B.R. provided a key observation that lymphotoxin could contribute to TNF-independent death in this model. B.R and L.S. critically reviewed the manuscript and provided helpful discussion. M.G.K performed the statistical analyses and wrote the manuscript with editing from I.R., E.M, B.A.M, A.M., and input from all co-authors.

Acknowledgements

20

Competing Financial Interests

A.Marson is a compensated co-founder, member of the boards of directors, and a member of the scientific advisory boards of Spotlight Therapeutics and Arsenal Biosciences. A.Marson was a compensated member of the scientific advisory board at PACT Pharma and was a compensated advisor to Juno Therapeutics and Trizell. A.Marson owns stock in Arsenal Biosciences, Spotlight Therapeutics, and PACT Pharma. A.Marson has received fees from Merck and Vertex and is an investor in and informal advisor to Offline Ventures. The Marson lab has received research support from Juno Therapeutics, Epinomics, Sanofi, GlaxoSmithKline, Gilead, and Anthem. The Kattah lab receives research support from Eli Lilly. The authors have no additional financial interests.

References

1. Hagiwara C, Tanaka M, Kudo H. Increase in colorectal epithelial apoptotic cells in patients with ulcerative colitis ultimately requiring surgery.. *Journal of gastroenterology and hepatology* 2002;17(7):758–764.

2. Zeissig S et al. Downregulation of epithelial apoptosis and barrier repair in active Crohn's disease by tumour necrosis factor alpha antibody treatment.. *Gut* 2004;53(9):1295–1302.

3. Kaser A, Zeissig S, Blumberg RS. Inflammatory Bowel Disease. *Annual Review of Immunology* 2010;28(1):573–621.

4. Goll R, Granlund A van B. Intestinal barrier homeostasis in inflammatory bowel disease. *Scandinavian Journal of Gastroenterology* 2014;50(1):3–12.

5. Hooper LV. Epithelial cell contributions to intestinal immunity.. *Advances in immunology* 2015;126:129–172.

6. Wlodarska M, Kostic AD, Xavier RJ. An Integrative View of Microbiome-Host Interactions in Inflammatory Bowel Diseases. *Cell Host and Microbe* 2015;17(5):577–591.

21

7. Adolph TE et al. Paneth cells as a site of origin for intestinal inflammation. *Nature* 2013;503(7475):272–276.

8. Matsuzawa-Ishimoto Y et al. Autophagy protein ATG16L1 prevents necroptosis in the intestinal epithelium.. *The Journal of experimental medicine* 2017;214(12):3687–3705.

9. Kattah MG et al. A20 and ABIN-1 synergistically preserve intestinal epithelial cell survival. *Journal of Experimental Medicine* 2018;265:jem.20180198-14.

10. Kinchen J et al. Structural Remodeling of the Human Colonic Mesenchyme in Inflammatory Bowel Disease.. *Cell* 2018;175(2):372-386.e17.

11. Parikh K et al. Colonic epithelial cell diversity in health and inflammatory bowel disease.. *Nature* 2019;567(7746):49–55.

12. Smillie CS et al. Intra- and Inter-cellular Rewiring of the Human Colon during Ulcerative Colitis. *Cell* 2019;178(3):714-730.e22.

13. Ma A, Malynn BA. A20: linking a complex regulator of ubiquitylation to immunity and human disease. *Nature Reviews Immunology* 2012;1–12.

14. Jostins L et al. Host-microbe interactions have shaped the genetic architecture of inflammatory bowel disease.. *Nature* 2012;491(7422):119–124.

15. Wang S, Wen F, Wiley GB, Kinter MT, Gaffney PM. An Enhancer Element Harboring Variants Associated with Systemic Lupus Erythematosus Engages the TNFAIP3 Promoter to Influence A20 Expression. *PLoS Genetics* 2013;9(9):e1003750-10.

16. Catrysse L et al. A20 prevents chronic liver inflammation and cancer by protecting hepatocytes from death.. *Cell Death and Disease* 2016;7(6):e2250–e2250.

17. Narzo AFD et al. Blood and Intestine eQTLs from an Anti-TNF-Resistant Crohn's Disease Cohort Inform IBD Genetic Association Loci.. *Clinical and translational gastroenterology* 2016;7(6):e177–e177.

18. Zhou Q et al. Biallelic hypomorphic mutations in a linear deubiquitinase define otulipenia, an early-onset autoinflammatory disease.. *Proceedings of the National Academy of Sciences of the United States of America* 2016;113(36):10127–10132.

19. Berteau F et al. Autosomic dominant familial Behçet disease and haploinsufficiency A20: A review of the literature. *Autoimmunity Reviews* 2018;17(8):809–815.

20. Razani B, Malynn BA, Ma A. Preserving immune homeostasis with A20 [Internet]. In: *Advances in Immunology*. Elsevier; 2020:1–48

21. Taniguchi K et al. Novel TNFAIP3 microdeletion in a girl with infantile-onset inflammatory bowel disease complicated by a severe perianal lesion. *Hum Genome Var* 2021;8(1):1.

22. Opipari AW, Hu HM, Yabkowitz R, Dixit VM. The A20 zinc finger protein protects cells from tumor necrosis factor cytotoxicity.. *Journal of Biological Chemistry* 1992;267(18):12424–12427.

23. Heyninck K et al. The zinc finger protein A20 inhibits TNF-induced NF-kappaB-dependent gene expression by interfering with an RIP- or TRAF2-mediated transactivation signal and directly binds to a novel NF-kappaB-inhibiting protein ABIN.. *The Journal of Cell Biology* 1999;145(7):1471–1482.

24. Lee EG. Failure to Regulate TNF-Induced NF-kappa B and Cell Death Responses in A20-Deficient Mice. *Science* 2000;289(5488):2350–2354.

25. Boone DL et al. The ubiquitin-modifying enzyme A20 is required for termination of Toll-like receptor responses. *Nature Immunology* 2004;5(10):1052–1060.

26. Wertz IE et al. De-ubiquitination and ubiquitin ligase domains of A20 downregulate NF-kappaB signalling.. *Nature* 2004;430(7000):694–699.

27. Wagner S et al. Ubiquitin binding mediates the NF-kappaB inhibitory potential of ABIN proteins.. *Oncogene* 2008;27(26):3739–3745.

28. Oshima S et al. ABIN-1 is a ubiquitin sensor that restricts cell death and sustains embryonic development. *Nature* 2009;457(7231):906–909.

29. Skaug B et al. Direct, noncatalytic mechanism of IKK inhibition by A20.. *Molecular Cell* 2011;44(4):559–571.

30. Bosanac I et al. Ubiquitin binding to A20 ZnF4 is required for modulation of NF-κB signaling.. *Molecular Cell* 2010;40(4):548–557.

31. Nanda SK et al. Polyubiquitin binding to ABIN1 is required to prevent autoimmunity.. *The Journal of experimental medicine* 2011;208(6):1215–1228.

32. Tokunaga F et al. Specific recognition of linear polyubiquitin by A20 zinc finger 7 is involved in NF-κB regulation.. *The EMBO journal* 2012;31(19):3856–3870.

33. Verhelst K et al. A20 inhibits LUBAC-mediated NF-κB activation by binding linear polyubiquitin chains via its zinc finger 7.. *The EMBO journal* 2012;31(19):3845–3855.

34. Lu TT et al. Dimerization and Ubiquitin Mediated Recruitment of A20, a Complex Deubiquitinating Enzyme. *Immunity* 2013;1–10.

35. Duong BH et al. A20 Restricts Ubiquitination of Pro-Interleukin-1β Protein Complexes and Suppresses NLRP3 Inflammasome Activity. *Immunity* 2015;42(1):55–67.

36. Wertz IE et al. Phosphorylation and linear ubiquitin direct A20 inhibition of inflammation. *Nature* 2015;528(7582):370–375.

37. Razani B et al. Non-catalytic ubiquitin binding by A20 prevents psoriatic arthritis–like disease and inflammation. *Nat Immunol* 2020;21(4):422–433.

38. Vereecke L et al. Enterocyte-specific A20 deficiency sensitizes to tumor necrosis factor-induced toxicity and experimental colitis.. *The Journal of experimental medicine* 2010;207(7):1513–1523.

39. Shao L et al. A20 Restricts Wnt Signaling in Intestinal Epithelial Cells and Suppresses Colon Carcinogenesis. *PLoS ONE* 2013;8(5):e62223.

40. Vereecke L et al. A20 controls intestinal homeostasis through cell-specific activities.. *Nature Communications* 2014;5:5103–12.

41. Feoktistova M et al. cIAPs block Ripoptosome formation, a RIP1/caspase-8 containing intracellular cell death complex differentially regulated by cFLIP isoforms.. *Molecular Cell* 2011;43(3):449–463.

42. Tenev T et al. The Ripoptosome, a Signaling Platform that Assembles in Response to Genotoxic Stress and Loss of IAPs. *Molecular Cell* 2011;43(3):432–448.

43. Dannappel M et al. RIPK1 maintains epithelial homeostasis by inhibiting apoptosis and necroptosis. *Nature* 2014;513(7516):90–94.

44. Günther C et al. Caspase-8 controls the gut response to microbial challenges by Tnf-α-dependent and independent pathways.. *Gut* 2015;64(4):601–610.

45. Vlantis K et al. NEMO Prevents RIP Kinase 1-Mediated Epithelial Cell Death and Chronic Intestinal Inflammation by NF-κB-Dependent and -Independent Functions. *Immunity* 2016;44(3):553–567.

46. Schwarzer R, Jiao H, Wachsmuth L, Tresch A, Pasparakis M. FADD and Caspase-8 Regulate Gut Homeostasis and Inflammation by Controlling MLKL- and GSDMD-Mediated Death of Intestinal Epithelial Cells. *Immunity* [published online ahead of print: 2020]; doi:10.1016/j.immuni.2020.04.002

47. Singh S, Fumery M, Sandborn WJ, Murad MH. Systematic review and network meta-analysis: first- and second-line biologic therapies for moderate-severe Crohn's disease. *Aliment Pharmacol Ther* 2018;48(4):394–409.

48. Feuerstein JD et al. AGA Clinical Practice Guidelines on the Management of Moderate to Severe Ulcerative Colitis. *Gastroenterology* 2020;158(5):1450–1461.

49. Singh S, Murad MH, Fumery M, Dulai PS, Sandborn WJ. First- and Second-Line Pharmacotherapies for Patients With Moderate to Severely Active Ulcerative Colitis: An Updated Network Meta-Analysis. *Clinical Gastroenterology and Hepatology* 2020;18(10):2179-2191.e6.

50. Nguyen NH, Singh S, Sandborn WJ. Positioning Therapies in the Management of Crohn's Disease. *Clinical Gastroenterology and Hepatology* 2020;18(6):1268–1279.

51. Alsina-Sanchis E et al. Intraperitoneal Oil Application Causes Local Inflammation with Depletion of Resident Peritoneal Macrophages. *Mol Cancer Res* 2021;19(2):288–300.

52. Chen S, Lee B, Lee AY-F, Modzelewski AJ, He L. Highly Efficient Mouse Genome Editing by CRISPR Ribonucleoprotein Electroporation of Zygotes. *Journal of Biological Chemistry* 2016;291(28):14457–14467.

53. Rakoff-Nahoum S, Paglino J, Eslami-Varzaneh F, Edberg S, Medzhitov R. Recognition of Commensal Microflora by Toll-Like Receptors Is Required for Intestinal Homeostasis. *Cell* 2004;118(2):229–241.

54. Asquith MJ, Boulard O, Powrie F, Maloy KJ. Pathogenic and Protective Roles of MyD88 in Leukocytes and Epithelial Cells in Mouse Models of Inflammatory Bowel Disease. *Gastroenterology* 2010;139(2):519-529.e2.

55. Frantz AL et al. Targeted deletion of MyD88 in intestinal epithelial cells results in compromised antibacterial immunity associated with downregulation of polymeric immunoglobulin receptor, mucin-2, and antibacterial peptides. *Mucosal Immunology* 2012;5(5):501–512.

56. West AP, Koblansky AA, Ghosh S. Recognition and signaling by toll-like receptors.. *Annual review of cell and developmental biology* 2006;22(1):409–437.

57. Dinarello CA. Immunological and Inflammatory Functions of the Interleukin-1 Family. *Annu. Rev. Immunol.* 2009;27(1):519–550.

58. Kaiser WJ, Offermann MK. Apoptosis Induced by the Toll-Like Receptor Adaptor TRIF Is Dependent on Its Receptor Interacting Protein Homotypic Interaction Motif. *J Immunol* 2005;174(8):4942–4952.

59. He S, Liang Y, Shao F, Wang X. Toll-like receptors activate programmed necrosis in macrophages through a receptor-interacting kinase-3-mediated pathway. *Proceedings of the National Academy of Sciences* 2011;108(50):20054–20059.

60. Kaiser WJ et al. Toll-like Receptor 3-mediated Necrosis via TRIF, RIP3, and MLKL. *Journal of Biological Chemistry* 2013;288(43):31268–31279.

61. Estornes Y et al. dsRNA induces apoptosis through an atypical death complex associating TLR3 to caspase-8. *Cell Death Differ* 2012;19(9):1482–1494.

62. Onizawa M et al. The ubiquitin-modifying enzyme A20 restricts ubiquitination of the kinase RIPK3 and protects cells from necroptosis. *Nature Immunology* 2015;16(6):618–627.

63. Chaturvedi MM, LaPushin R, Aggarwal BB. Tumor necrosis factor and lymphotoxin. Qualitative and quantitative differences in the mediation of early and late cellular response.. *Journal of Biological Chemistry* 1994;269(20):14575–14583.

64. Bossen C et al. Interactions of Tumor Necrosis Factor (TNF) and TNF Receptor Family Members in the Mouse and Human. *Journal of Biological Chemistry* 2006;281(20):13964–13971.

65. Etemadi N et al. Lymphotoxin α induces apoptosis, necroptosis and inflammatory signals with the same potency as tumour necrosis factor. *The FEBS Journal* 2013;280(21):5283–5297.

66. Chiang EY et al. Targeted depletion of lymphotoxin-α–expressing TH1 and TH17 cells inhibits autoimmune disease. *Nature Medicine* 2009;15(7):766–773.

67. Dondelinger Y et al. RIPK3 contributes to TNFR1-mediated RIPK1 kinase-dependent apoptosis in conditions of cIAP1/2 depletion or TAK1 kinase inhibition.. *Cell death and differentiation* 2013;20(10):1381–1392.

68. Kondylis V, Kumari S, Vlantis K, Pasparakis M. The interplay of IKK, NF-κB and RIPK1 signaling in the regulation of cell death, tissue homeostasis and inflammation. *Immunol Rev* 2017;277(1):113–127.

69. Takahashi N et al. Necrostatin-1 analogues: critical issues on the specificity, activity and in vivo use in experimental disease models. *Cell Death and Disease* 2012;3(11):e437-10.

70. Kaiser WJ et al. RIP3 mediates the embryonic lethality of caspase-8-deficient mice. *Nature* 2011;471(7338):368–372.

71. Oberst A et al. Catalytic activity of the caspase-8–FLIPL complex inhibits RIPK3-dependent necrosis. *Nature* 2011;471(7338):363–367.

72. Günther C et al. Caspase-8 regulates TNF-α-induced epithelial necroptosis and terminal ileitis. *Nature* 2011;477(7364):335–339.

73. Tam V et al. Benefits and limitations of genome-wide association studies. *Nat Rev Genet* 2019;20(8):467–484.

74. Nenci A et al. Epithelial NEMO links innate immunity to chronic intestinal inflammation. *Nature* 2007;446(7135):557–561.

75. Welz P-S et al. FADD prevents RIP3-mediated epithelial cell necrosis and chronic intestinal inflammation. *Nature* 2011;477(7364):330–334.

76. Takahashi N et al. RIPK1 ensures intestinal homeostasis by protecting the epithelium against apoptosis. *Nature* 2014;513(7516):95–99.

77. Wang R et al. Gut stem cell necroptosis by genome instability triggers bowel inflammation. *Nature* 2020;580(7803):386–390.

78. Yang D et al. ZBP1 mediates interferon-induced necroptosis. *Cell Mol Immunol* 2020;17(4):356–368.

79. Upton JW, Kaiser WJ, Mocarski ES. DAI/ZBP1/DLM-1 Complexes with RIP3 to Mediate Virus-Induced Programmed Necrosis that Is Targeted by Murine Cytomegalovirus vIRA. *Cell Host & Microbe* 2012;11(3):290–297.

80. Lin J et al. RIPK1 counteracts ZBP1-mediated necroptosis to inhibit inflammation. *Nature* 2016;540(7631):124–128.

81. Walle LV et al. Negative regulation of the NLRP3 inflammasome by A20 protects against arthritis. *Nature* 2014;512(7512):69–73.

82. Broz P, Dixit VM. Inflammasomes: mechanism of assembly, regulation and signalling. *Nature Reviews Immunology* 2016;16(7):407–420.

83. Kayagaki N et al. Caspase-11 cleaves gasdermin D for non-canonical inflammasome signalling.. *Nature* 2015;526(7575):666–671.

84. Shi J et al. Cleavage of GSDMD by inflammatory caspases determines pyroptotic cell death. *Nature* 2015;526(7575):660–665.

85. Kang T-B, Yang S-H, Toth B, Kovalenko A, Wallach D. Caspase-8 Blocks Kinase RIPK3-Mediated Activation of the NLRP3 Inflammasome. *Immunity* 2013;38(1):27–40.

86. Lawlor KE et al. RIPK3 promotes cell death and NLRP3 inflammasome activation in the absence of MLKL. *Nat Commun* 2015;6(1):6282.

87. Orning P et al. Pathogen blockade of TAK1 triggers caspase-8–dependent cleavage of gasdermin D and cell death. *Science* 2018;362(6418):1064–1069.

88. Sarhan J et al. Caspase-8 induces cleavage of gasdermin D to elicit pyroptosis during Yersinia infection.. *Proceedings of the National Academy of Sciences of the United States of America* 2018;115(46):E10888–E10897.

89. Fritsch M et al. Caspase-8 is the molecular switch for apoptosis, necroptosis and pyroptosis. *Nature* 2019;575(7784):683–687.

90. Newton K et al. Activity of caspase-8 determines plasticity between cell death pathways. *Nature* 2019;575(7784):679–682.

91. Dideberg V et al. Lymphotoxin alpha gene in Crohn's disease patients: absence of implication in the response to infliximab in a large cohort study. *Pharmacogenetics and Genomics* 2006;16(5):369–373.

92. Sandborn WJ et al. Etanercept for active Crohn's disease: A randomized, double-blind, placebo-controlled trial. *Gastroenterology* 2001;121(5):1088–1094.

93. Mitoma H et al. Mechanisms for cytotoxic effects of anti–tumor necrosis factor agents on transmembrane tumor necrosis factor α–expressing cells: Comparison among infliximab, etanercept, and adalimumab. *Arthritis Rheum* 2008;58(5):1248–1257.

94. Mitoma H, Horiuchi T, Tsukamoto H, Ueda N. Molecular mechanisms of action of anti-TNF-α agents – Comparison among therapeutic TNF-α antagonists. *Cytokine* 2018;101:56–63.

95. Sheehy C, Murphy E, Barry M. Effective co-administration of infliximab and etanercept following the failure of sequential anti-TNF agents in a patient with HLA-B27-associated arthropathy. *Rheumatology* 2006;45(10):1314–1315.

96. Bank S et al. Genetically determined high activity of IL-12 and IL-18 in ulcerative colitis and TLR5 in Crohns disease were associated with non-response to anti-TNF therapy. *Pharmacogenomics J* 2018;18(1):87–97.

97. Martin JC et al. Single-Cell Analysis of Crohn's Disease Lesions Identifies a Pathogenic Cellular Module Associated with Resistance to Anti-TNF Therapy. *Cell* 2019;178(6):1493-1508.e20.

98. Mitsialis V et al. Single-Cell Analyses of Colon and Blood Reveal Distinct Immune Cell Signatures of Ulcerative Colitis and Crohn's Disease. *Gastroenterology* [published online ahead of print: 2020]; doi:10.1053/j.gastro.2020.04.074

99. Tavares RM et al. The Ubiquitin Modifying Enzyme A20 Restricts B Cell Survival and Prevents Autoimmunity. *Immunity* 2010;33(2):181–191.

100. Marjou FE et al. Tissue-specific and inducible Cre-mediated recombination in the gut epithelium. *genesis* 2004;39(3):186–193.

101. Sato T, Clevers H. Primary Mouse Small Intestinal Epithelial Cell Cultures. In: Humana Press; 2012:319–328

102. Erben U et al. A guide to histomorphological evaluation of intestinal inflammation in mouse models.. *International journal of clinical and experimental pathology* 2014;7(8):4557–4576.

Figure Legends

Figure 1. Germ-free *A20/Abin-1*$^{T-\Delta IEC}$*Tnf*$^{-/-}$ mice are protected from TNF-independent apoptotic IEC death *in vivo*. (A) Kaplan-Meier survival curves of the indicated genotypes of tamoxifen-treated mice. **(B)** Kaplan-

Meier survival curves of tamoxifen-treated mice with the indicated genotypes, either germ-free or conventionalized with cecal contents from SPF mice (GF-CONV). (**C**) Representative H&E images, (**D**) histological scoring, (**E**) representative CC3 IHC images, and (**F**) CC3+ cells per crypt of small intestine and colon sections 40h after tamoxifen treatment in mice with the indicated genotype; each data point represents one mouse (mean ± SEM). The legend for panel (**F**) is shown in panel (**D**). For panels (**A,B**), statistical significance between *A20/Abin-1$^{T-ΔIEC}$* and *A20/Abin-1$^{T-ΔIEC}$Tnf$^{-/-}$* mice was assessed by Log-rank Mantel-Cox test. For panels (**D**) and (**F**), significance was assessed by one-way ANOVA with Tukey's multiple comparison test. Only significant differences are shown; *=p<0.05, **=p<0.01, ***=p < 0.001; ****=p< 0.0001. Scale bars, 100μm. Data represent at least two independent experiments.

Figure 2. Deletion of *MyD88* significantly improves survival, reduces epithelial injury, and decreases IEC apoptosis in *A20/Abin-1$^{T-ΔIEC}$Tnf$^{-/-}$* mice. (**A**) Agarose gel electrophoresis and (**B**) immunoblot of splenocyte lysates from *A20/Abin-1$^{T-ΔIEC}$Tnf$^{-/-}$* mice with the indicated *MyD88* genotypes. (**C**). Kaplan-Meier survival curves of the indicated genotypes of tamoxifen-treated mice. (**D**) Representative H&E images, (**E**) histological scoring, (**F**) representative CC3 IHC images, and (**G**) CC3+ cells per crypt of small intestine and colon sections 40h after tamoxifen treatment in mice with the indicated genotype; each data point represents one mouse (mean ± SEM). The legend for panel (**G**) is shown in panel (**E**). For panel (**C**), statistical significance comparing *A20/Abin-1$^{T-ΔIEC}$Tnf$^{-/-}$MyD88$^{+/+}$* mice to *MyD88$^{-/-}$* and *MyD88$^{+/-}$* mice was assessed by Log-rank Mantel-Cox test. For panels (**E**) and (**G**), statistical significance was assessed by one-way ANOVA with Tukey's multiple comparison test. Only significant differences are shown; *=p<0.05, **=p<0.01, ***=p < 0.001; ****=p< 0.0001. Scale bars, 100μm. Data represent at least two independent experiments.

Figure 3. Deletion of *Trif* partially improves survival and modestly reduces IEC apoptosis in *A20/Abin-1$^{T-ΔIEC}$Tnf$^{-/-}$* mice. (**A**) Quantitative luminescent cell viability assay of enteroid cultures with the indicated genotype treated with the indicated stimuli (mean ± SEM; pam3CSK4 500ng/ml; poly (I:C) 25ug/ml; IL-1β 25ng/ml; LPS 500ng/ml). (**B**). Kaplan-Meier survival curves of the indicated genotypes of tamoxifen-treated mice. (**C**) Representative H&E images, (**D**) histological scoring, (**E**) representative CC3 IHC images, and (**F**) CC3+ cells per crypt of small intestine and colon sections 40h after tamoxifen treatment in mice with the indicated genotype; each data point represents one mouse (mean ± SEM). The legend for panel (**F**) is shown in panel (**D**). For panel (A), statistical significance was assessed using two-way ANOVA with Bonferroni's

multiple comparison test. For panel (**B**), significance was comparing *A20/Abin-1*$^{T\text{-}\Delta IEC}$*Tnf*$^{-/-}$*Trif*$^{+/+}$ mice to *Trif*$^{-/-}$

and *Trif*$^{+/-}$ mice was assessed by Log-rank Mantel-Cox test. For panels (**D**) and (**F**), statistical significance was

assessed by one-way ANOVA with Tukey's multiple comparison test. Only significant differences are shown;

*=p<0.05, **=p<0.01, ***=p < 0.001; ****=p< 0.0001. Scale bars, 100μm. Data represent at least two

independent experiments.

Figure 4. Combined deletion of *Ripk3 and Casp8* completely protects against death, epithelial injury,

and IEC apoptosis in *A20/Abin-1*$^{T\text{-}\Delta IEC}$ mice. (**A**). Kaplan-Meier survival curves of the indicated genotypes of

tamoxifen-treated mice. (**B**) Representative H&E images, (**C**) histological scoring, (**D**) representative CC3 IHC

images, and (**F**) CC3+ cells per crypt of small intestine and colon sections 40h after tamoxifen treatment in

mice with the indicated genotype; each data point represents one mouse (mean ± SEM). The legend for panel

(**E**) is shown in panel (**C**). (**F**) Quantitative luminescent cell viability assay of enteroids with the indicated

genotype treated with indicated stimuli (mean ± SEM). For panel (**A**), statistical significance comparing

A20/Abin-1$^{T\text{-}\Delta IEC}$*Ripk3*$^{-/-}$*Casp8*$^{+/+}$ mice to *Casp8*$^{+/-}$ and *Casp8*$^{-/-}$ mice was assessed by Log-rank Mantel-Cox

test. For panels (**C**), (**E**), and (**F**), statistical significance was assessed by one-way ANOVA with Tukey's

multiple comparison test. Only significant differences are shown; *=p<0.05, **=p<0.01, ***=p < 0.001; ****=p<

0.0001. Scale bars, 100μm. Data represent at least two independent experiments.

Figure 5. LTα$_3$ induces death in *A20/Abin-1*$^{T\text{-}\Delta IEC}$*Tnf*$^{-/-}$ enteroids through activation of TNFR1. (A,B,D-G)

Quantitative luminescent cell viability assay of enteroids with the indicated genotype treated with indicated

stimuli (mean ± SEM; RANKL, LIGHT, TL1A, TNF 25ng/ml; hLTα$_3$ 5ng/ml; LTα$_1$β$_2$ 50ng/ml; anti-LTα and

isotype control 10ug/ml; TNFR1-Fc, LTBR-Fc 100ug/ml). (**C**) ELISA of undiluted conditioned media (CM) from

293T cells either mock transduced (Mock CM) or stably transduced with a mouse LTα$_3$-Fc expression

construct (LTα$_3$-Fc CM) with anti-mIgG2a capture and anti-LTα detection antibodies (mean ± SEM). For panel

(**A**), significance was assessed by one-way ANOVA with Dunnett's multiple comparison test relative to vehicle.

For panel (**B, E**), significance was assessed using two-way ANOVA with Tukey's multiple comparison test. For

panels (**C,D,F,G**), significance was assessed using one-way ANOVA with Tukey's multiple comparison test.

Only significant differences are shown; *=p<0.05, **=p<0.01, ***=p < 0.001; ****=p< 0.0001. Data represent at

least two independent experiments.

Figure 6. LTα$_3$ can induce both Casp8-dependent apoptosis and Ripk3-dependent necroptosis in

***A20/Abin-1$^{T-\Delta IEC}$Tnf$^{-/-}$* enteroids.** (**A**,**C**) Quantitative luminescent cell viability assay of enteroids with the

indicated genotypes treated with indicated stimuli (mean ± SEM; Nec1s, Emricasan 50μM; TNF 50ng/ml).

(**B**,**D**) Immunoblotting analyses of enteroid cultures with the indicated genotypes treated with 4-OHT for 24h

followed by recombinant hLTα$_3$ 20ng/ml for the indicated time, with or without 50μM Nec1s or 50μM emricasan

as indicated. Lysates were immunoblotted with the antibodies indicated on the right. Solid arrows indicate full-

length protein; open arrows indicate cleaved protein. For panel (**A**), significance was assessed using two-way

ANOVA with Dunnett's multiple comparison test relative to LTα$_3$-Fc CM. For panel (**C**), significance was

assessed by two-way ANOVA with Bonferroni's multiple comparison test comparing between genotypes for

each stimulation condition. Only significant differences are shown; *=p<0.05, **=p<0.01, ***=p < 0.001; ****=p<

0.0001. Data represent at least two independent experiments.

Figure 7. Intestinal *Lta* is increased in *A20/Abin-1$^{T-\Delta IEC}$Tnf$^{-/-}$* mice and anti-LTα improves survival in

***A20/Abin-1$^{T-\Delta IEC}$Tnf$^{-/-}$MyD88$^{+/+}$* and *MyD88$^{+/-}$* mice.** (**A**) Representative chromogenic RNA-ISH images of *Lta*,

(**B**) quantitation of *Lta* area, and (**C**) qPCR for *Lta* in small intestine and colon sections 40h after tamoxifen

treatment in mice with the indicated genotype; each data point represents one mouse (mean ± SEM). (**D**,**F**)

Weight curve and (**E**,**G**) Kaplan-Meier survival curves of the indicated genotypes of tamoxifen-treated mice

treated with anti-LTα or isotype control. For panel (**B**), statistical significance was assessed using two-way

ANOVA. For panel (**C**), significance was assessed using one-way ANOVA with Dunnett's multiple comparison

test relative to *A20/Abin-1$^{T-\Delta IEC}$Tnf$^{-/-}$* mice. For panels (**D**) and (**F**), significance was assessed by two-way

ANOVA with Bonferroni's multiple comparison test. For panels (**E**) and (**G**), significance was assessed by Log-

rank Mantel-Cox test. Only significant differences are shown; *=p<0.05, **=p<0.01, ***=p < 0.001; ****=p<

0.0001. Scale bars, 50μm. Data represent at least two independent experiments.

Supplemental Material:

Supplemental Figure 1 shows tamoxifen-induced deletion of floxed A20 and ABIN-1 on a *Vil-cre-ER^{T2+}*

background *in vivo* and *in vitro*.

Supplemental Figure 2 shows the sequence of edited *MyD88* in *A20/Abin-1$^{T-\Delta IEC}$Tnf$^{-/-}$* mice.

Supplemental Figure 3 shows IL18 stimulation of *A20/Abin-1$^{T-\Delta IEC}$Tnf$^{-/-}$* enteroids and editing of *Trif* in

A20/Abin-1$^{T-\Delta IEC}$Tnf$^{-/-}$ mice.

Supplemental Figure 4 shows deletion of *Casp8* in *A20/Abin-1*$^{T-\Delta IEC}$*Ripk3*$^{-/-}$ mice and poly(I:C) stimulation of

A20/Abin-1$^{T-\Delta IEC}$*Ripk3*$^{-/-}$ and *A20/Abin-1*$^{T-\Delta IEC}$*Ripk3*$^{-/-}$*Casp8*$^{-/-}$ enteroids.
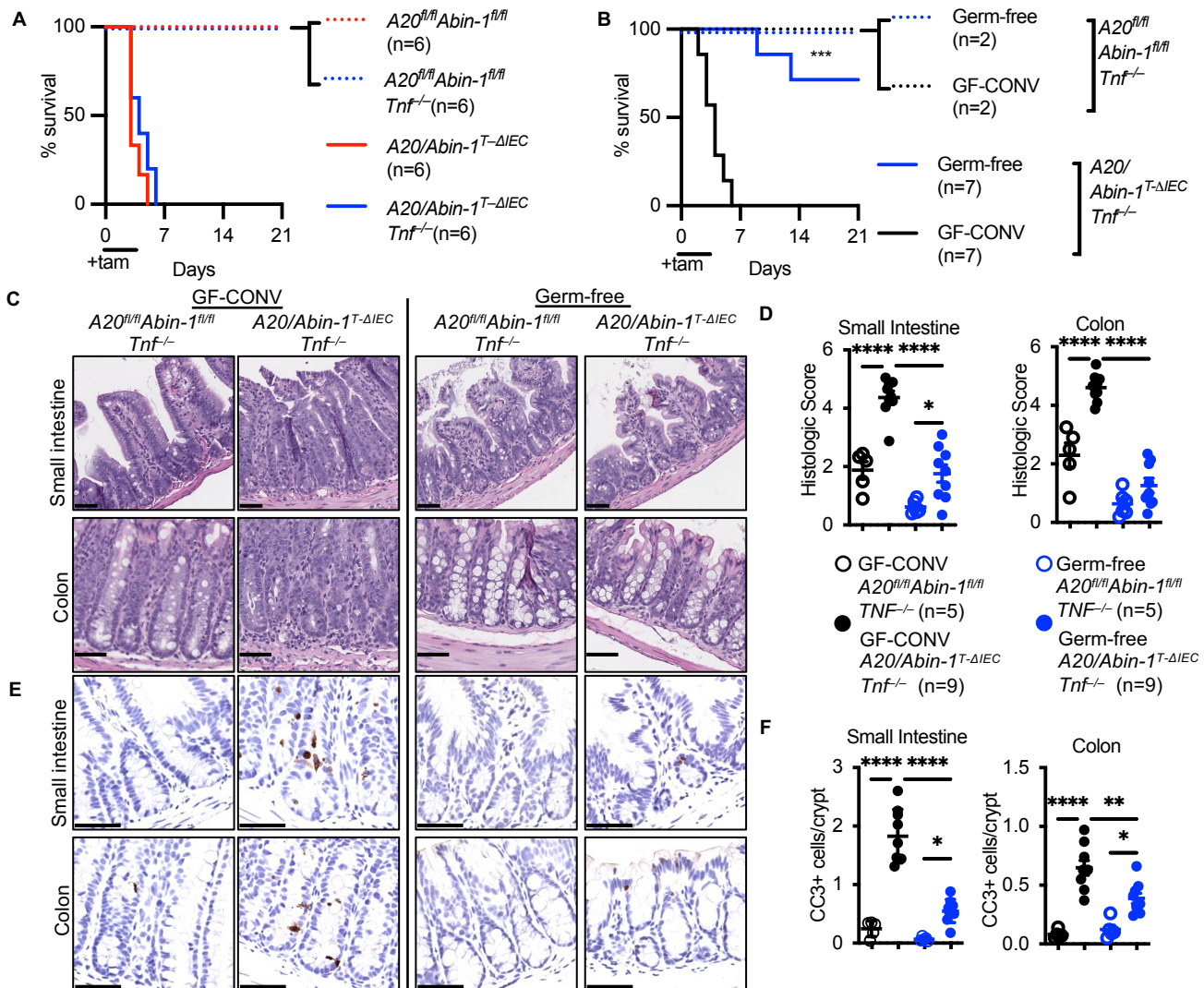
Figure 1

Figure 1. Germ-free $A20/Abin-1^{T-\Delta IEC}Tnf^{-/-}$ mice are protected from TNF-independent apoptotic IEC death in vivo. (**A**) Kaplan-Meier survival curves of the indicated genotypes of tamoxifen-treated mice. (**B**) Kaplan-Meier survival curves of tamoxifen-treated mice with the indicated genotypes, either germ-free or conventionalized with cecal contents from SPF mice (GF-CONV). (**C**) Representative H&E images, (**D**) histological scoring, (**E**) representative CC3 IHC images, and (**F**) CC3+ cells per crypt of small intestine and colon sections 40h after tamoxifen treatment in mice with the indicated genotype; each data point represents one mouse (mean ± SEM). The legend for panel (**F**) is shown in panel (**D**). For panels (**A,B**), statistical significance between $A20/Abin-1^{T-\Delta IEC}$ and $A20/Abin-1^{T-\Delta IEC}Tnf^{-/-}$ mice was assessed by Log-rank Mantel-Cox test. For panels (**D**) and (**F**), significance was assessed by one-way ANOVA with Tukey's multiple comparison test. Only significant differences are shown; *=p<0.05, **=p<0.01, ***=p < 0.001; ****=p< 0.0001. Scale bars, 100µm. Data represent at least two independent experiments.

Figure 2

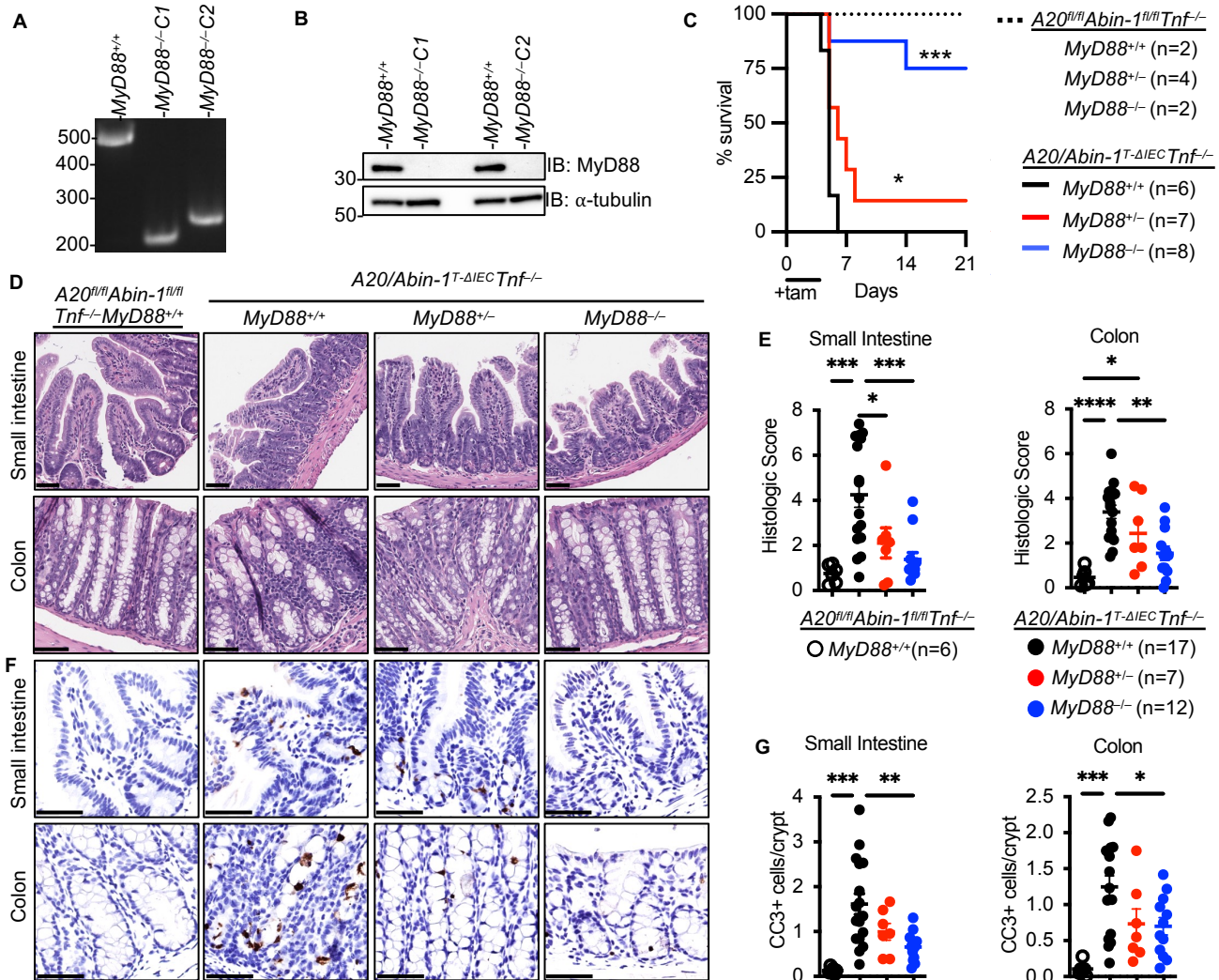**Figure 2. Deletion of *MyD88* significantly improves survival, reduces epithelial injury, and decreases IEC apoptosis in *A20/Abin-1^T-ΔIEC^Tnf^−/−* mice.** (**A**) Agarose gel electrophoresis and (**B**) immunoblot of splenocyte lysates from *A20/Abin-1^T-ΔIEC^Tnf^−/−* mice with the indicated *MyD88* genotypes. (**C**). Kaplan-Meier survival curves of the indicated genotypes of tamoxifen-treated mice. (**D**) Representative H&E images, (**E**) histological scoring, (**F**) representative CC3 IHC images, and (**G**) CC3+ cells per crypt of small intestine and colon sections 40h after tamoxifen treatment in mice with the indicated genotype; each data point represents one mouse (mean ± SEM). The legend for panel (**G**) is shown in panel (**E**). For panel (**C**), statistical significance comparing *A20/Abin-1^T-ΔIEC^Tnf^−/−^MyD88^+/+^* mice to *MyD88^−/−^* and *MyD88^+/−^* mice was assessed by Log-rank Mantel-Cox test. For panels (**E**) and (**G**), statistical significance was assessed by one-way ANOVA with Tukey's multiple comparison test. Only significant differences are shown; *=p<0.05, **=p<0.01, ***=p < 0.001; ****=p< 0.0001. Scale bars, 100μm. Data represent at least two independent experiments.

Figure 3

Figure 3. Deletion of *Trif* partially improves survival and modestly reduces IEC apoptosis in *A20/Abin-1^{T-ΔIEC}Tnf^{-/-}* mice. (A) Quantitative luminescent cell viability assay of enteroid cultures with the indicated genotype treated with the indicated stimuli (mean ± SEM; pam3CSK4 500ng/ml; poly (I:C) 25ug/ml; IL-1β 25ng/ml; LPS 500ng/ml). (**B**). Kaplan-Meier survival curves of the indicated genotypes of tamoxifen-treated mice. (**C**) Representative H&E images, (**D**) histological scoring, (**E**) representative CC3 IHC images, and (**F**) CC3+ cells per crypt of small intestine and colon sections 40h after tamoxifen treatment in mice with the indicated genotype; each data point represents one mouse (mean ± SEM). The legend for panel (**D**) is shown in panel (**F**). For panel (**A**), statistical significance was assessed using two-way ANOVA with Bonferroni's multiple comparison test. For panels (**D**) and (**F**), statistical significance was assessed by one-way ANOVA with Tukey's multiple comparison test. For panel (**B**), significance was comparing *A20/Abin-1^{T-ΔIEC}Tnf^{-/-}Trif^{+/+}* mice to *Trif^{-/-}* and *Trif^{+/-}* mice was assessed by Log-rank Mantel-Cox test. Only significant differences are shown; *=p<0.05, **=p<0.01, ***=p < 0.001; ****=p< 0.0001. Scale bars, 100μm. Data represent at least two independent experiments.
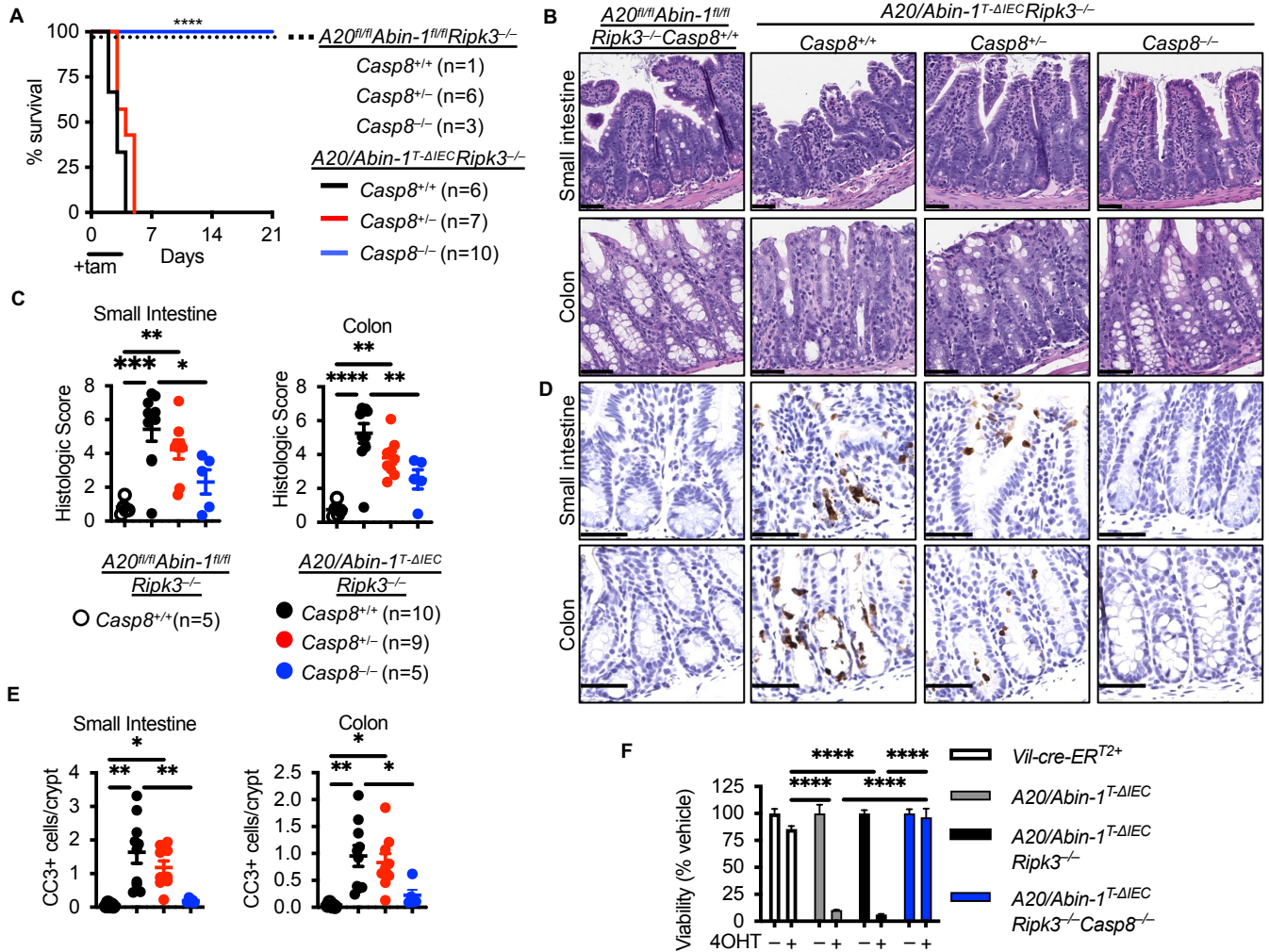
Figure 4

Figure 4. Combined deletion of *Ripk3 and Casp8* completely protects against death, epithelial injury, and IEC apoptosis in *A20/Abin-1^{T-ΔIEC}* mice. (**A**). Kaplan-Meier survival curves of the indicated genotypes of tamoxifen-treated mice. (**B**) Representative H&E images, (**C**) histological scoring, (**D**) representative CC3 IHC images, and (**F**) CC3+ cells per crypt of small intestine and colon sections 40h after tamoxifen treatment in mice with the indicated genotype; each data point represents one mouse (mean ± SEM). The legend for panel (**E**) is shown in panel (**C**). (**F**) Quantitative luminescent cell viability assay of enteroids with the indicated genotype treated with indicated stimuli (mean ± SEM). For panel (**A**), statistical significance comparing *A20/Abin-1^{T-ΔIEC}Ripk3^{-/-}Casp8^{+/+}* mice to *Casp8^{+/-}* and *Casp8^{-/-}* mice was assessed by Log-rank Mantel-Cox test. For panels (**C**), (**E**), and (**F**), statistical significance was assessed by one-way ANOVA with Tukey's multiple comparison test. Only significant differences are shown; *=p<0.05, **=p<0.01, ***=p < 0.001; ****=p< 0.0001. Scale bars, 100μm. Data represent at least two independent experiments.
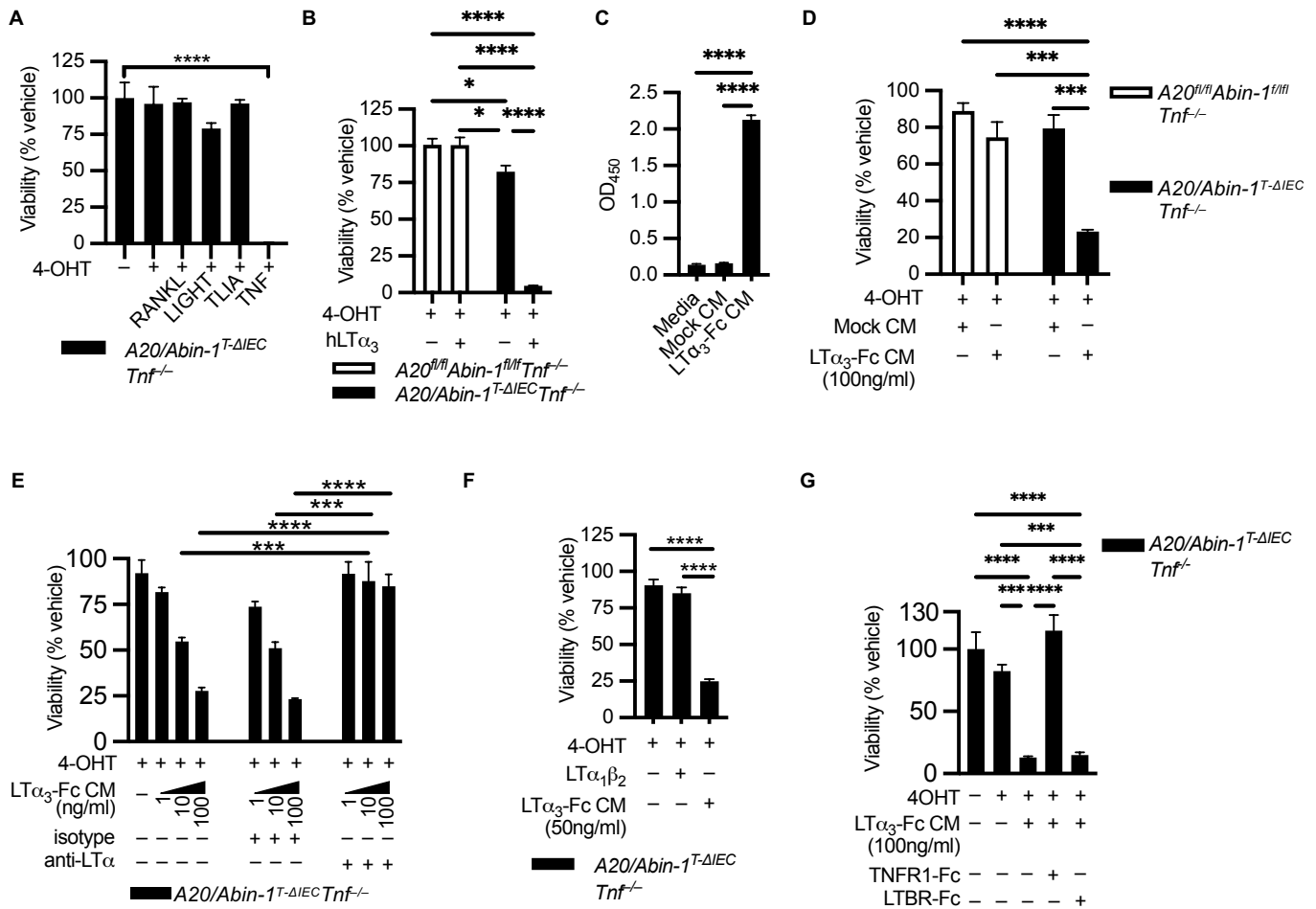
Figure 5

Figure 5. LTα₃ induces death in _A20/Abin-1^{T-ΔIEC}Tnf^{-/-}_ enteroids through activation of TNFR1. (**A**,**B**,**D-G**) Quantitative luminescent cell viability assay of enteroids with the indicated genotype treated with indicated stimuli (mean ± SEM; RANKL, LIGHT, TL1A, TNF 25ng/ml; hLTα₃ 5ng/ml; LTα₁β₂ 50ng/ml; anti-LTα and isotype control 10ug/ml; TNFR1-Fc, LTBR-Fc 100ug/ml). (**C**) ELISA of undiluted conditioned media (CM) from 293T cells either mock transduced (Mock CM) or stably transduced with a mouse LTα₃-Fc expression construct (LTα₃-Fc CM) with anti-mIgG2a capture and anti-LTα detection antibodies (mean ± SEM) . For panel (**A**), significance was assessed by one-way ANOVA with Dunnett's multiple comparison test relative to vehicle. For panel (**B, E**), significance was assessed using two-way ANOVA with Tukey's multiple comparison test. For panels (**C,D,F,G**), significance was assessed using one-way ANOVA with Tukey's multiple comparison test. Only significant differences are shown; *=p<0.05, **=p<0.01, ***=p < 0.001; ****=p< 0.0001. Data represent at least two independent experiments.
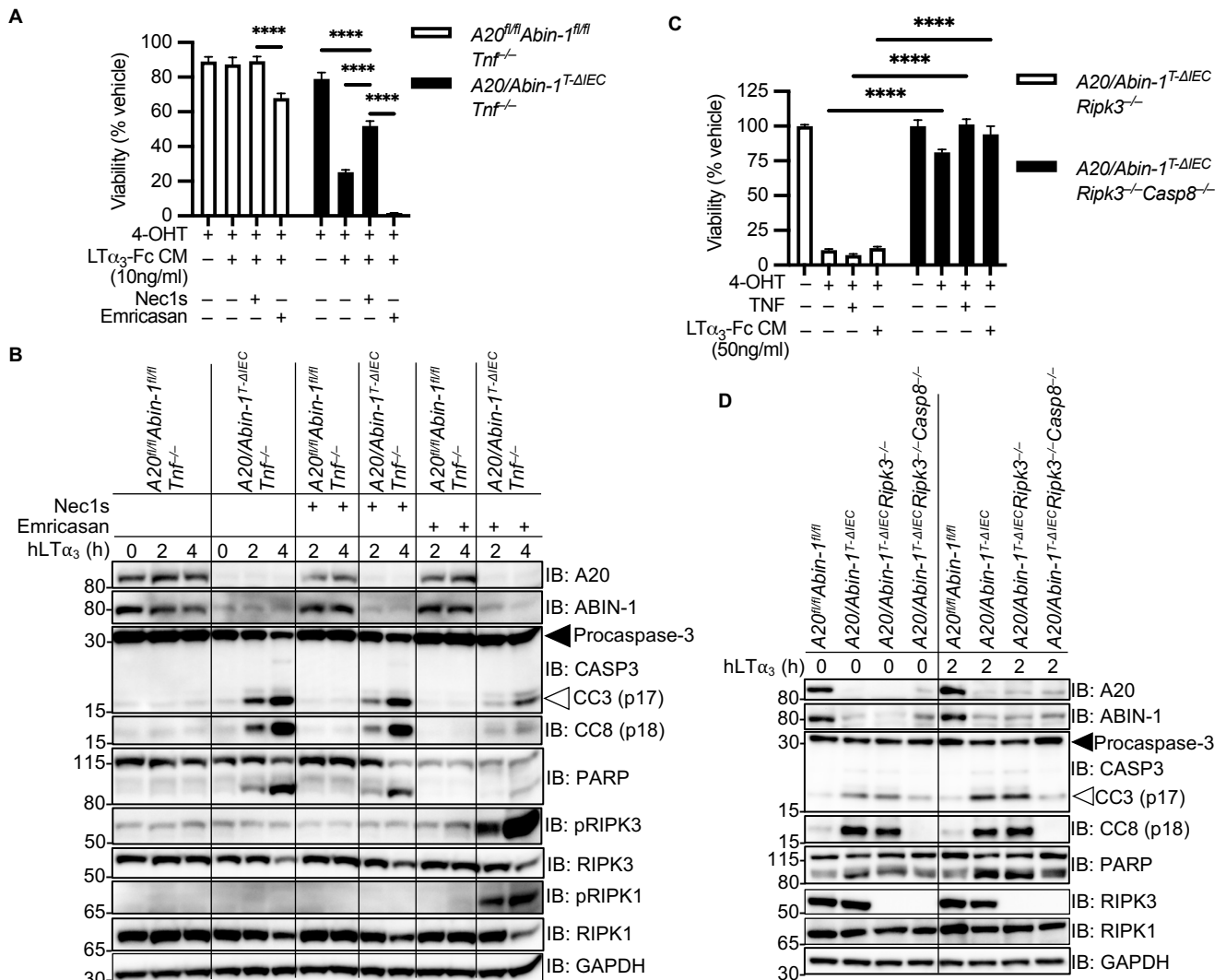
Figure 6

Figure 6. LTα₃ can induce both Casp8-dependent apoptosis and Ripk3-dependent necroptosis in *A20/Abin-1^T-ΔIEC Tnf^−/−* enteroids.
(**A**,**C**) Quantitative luminescent cell viability assay of enteroids with the indicated genotypes treated with indicated stimuli (mean ± SEM; Nec1s, Emricasan 50μM; TNF 50ng/ml). (**B**,**D**) Immunoblotting analyses of enteroid cultures with the indicated genotypes treated with 4-OHT for 24h followed by recombinant hLTα₃ 20ng/ml for the indicated time, with or without 50μM Nec1s or 50μM emricasan as indicated. Lysates were immunoblotted with the antibodies indicated on the right. Solid arrows indicate full-length protein; open arrows indicate cleaved protein. For panel (**A**), significance was assessed using two-way ANOVA with Dunnett's multiple comparison test relative to LTα₃-Fc CM. For panel (**C**), significance was assessed by two-way ANOVA with Bonferroni's multiple comparison test comparing between genotypes for each stimulation condition. Only significant differences are shown; *=p<0.05, **=p<0.01, ***=p < 0.001; ****=p< 0.0001. Data represent at least two independent experiments.
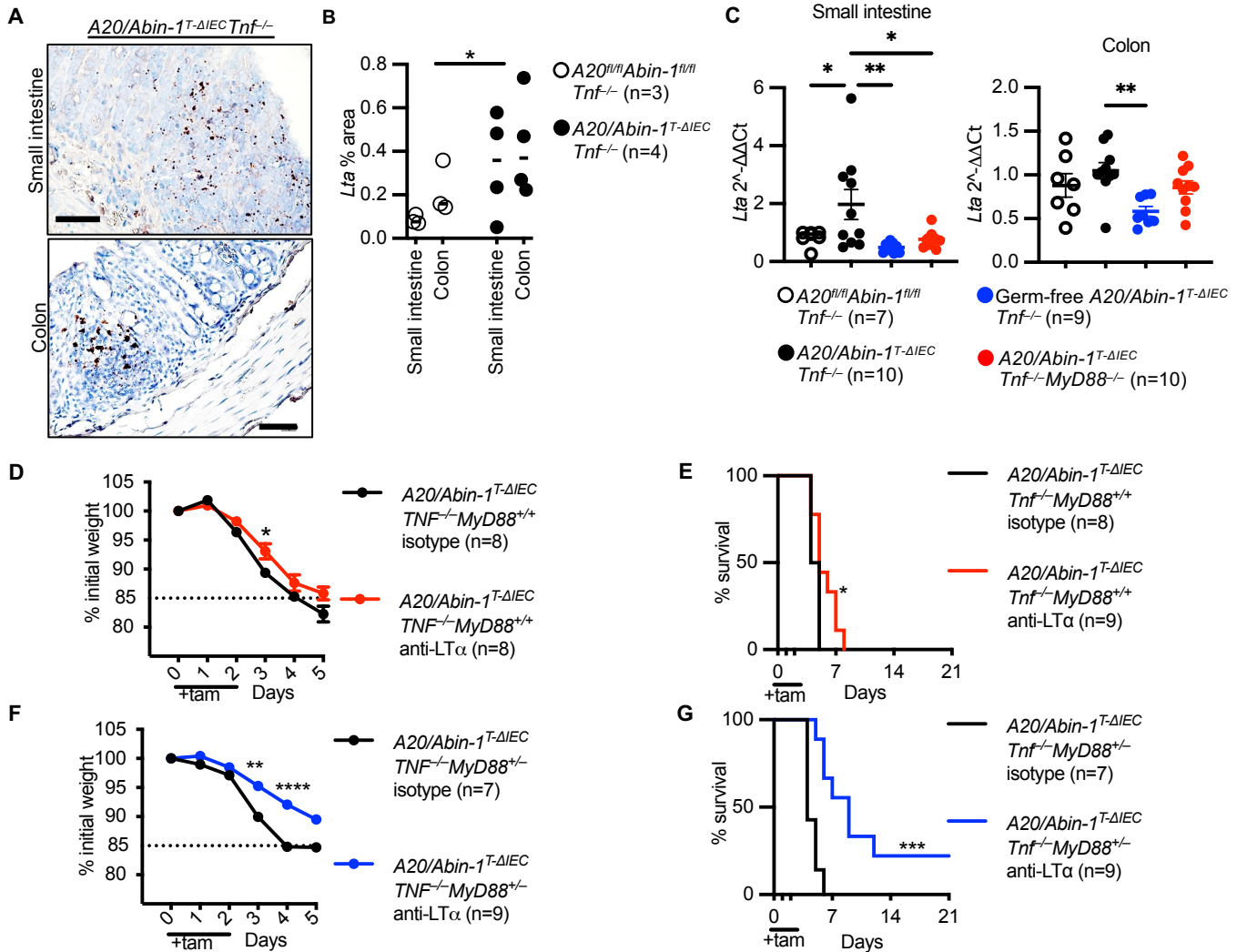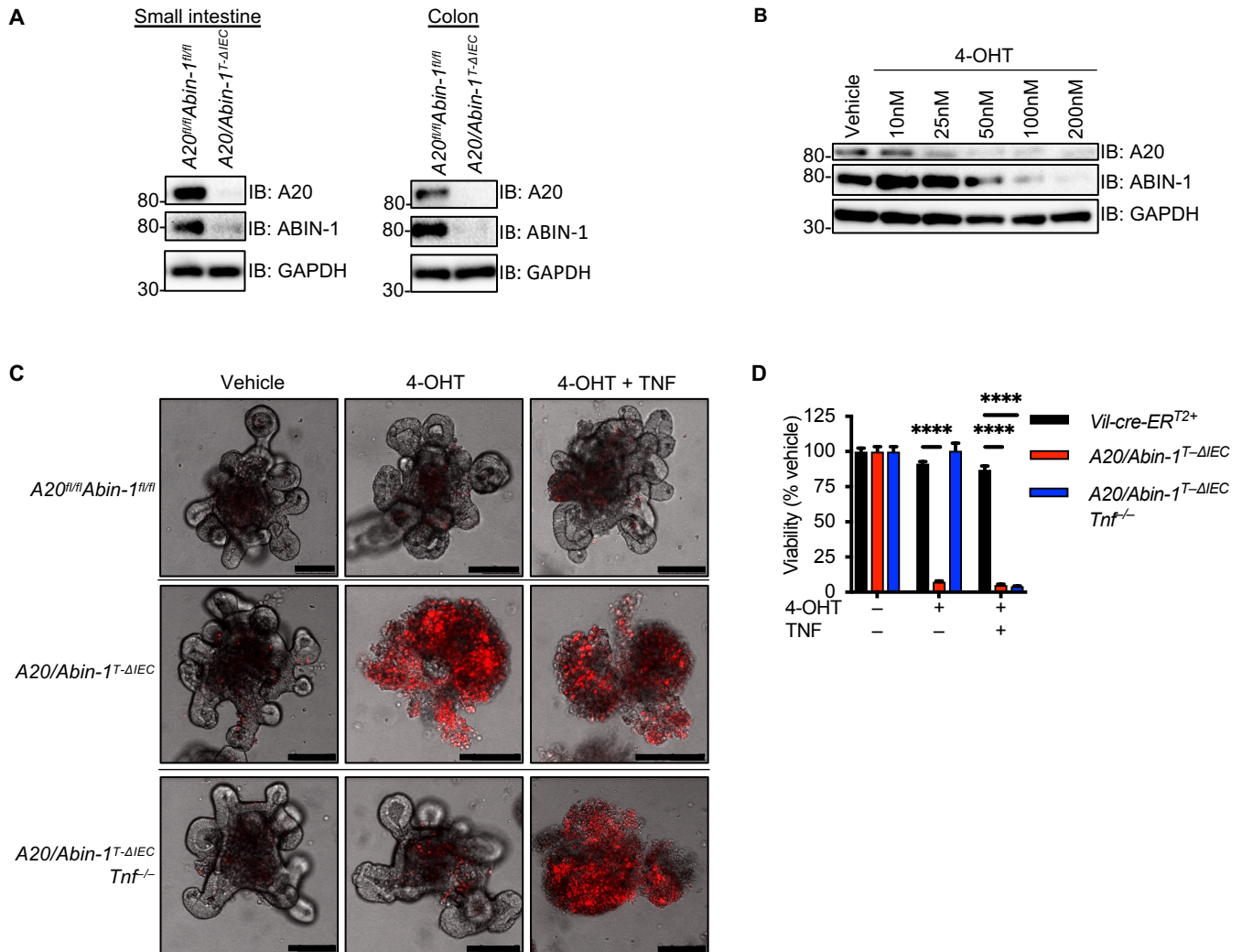
Figure 7

Figure 7. Intestinal *Lta* is increased in *A20/Abin-1$^{T-\Delta IEC}$Tnf$^{-/-}$* mice and anti-LTα improves survival in *A20/Abin-1$^{T-\Delta IEC}$Tnf$^{-/-}$MyD88$^{+/+}$* and *MyD88$^{+/-}$* mice. (**A**) Representative chromogenic RNA-ISH images of *Lta*, (**B**) quantitation of *Lta* area, and (**C**) qPCR for *Lta* in small intestine and colon sections 40h after tamoxifen treatment in mice with the indicated genotype; each data point represents one mouse (mean ± SEM). (**D,F**) Weight curve and (**E,G**) Kaplan-Meier survival curves of the indicated genotypes of tamoxifen-treated mice treated with anti-LTα or isotype control. For panel (**B**), statistical significance was assessed using two-way ANOVA. For panel (**C**), significance was assessed using one-way ANOVA with Dunnett's multiple comparison test relative to *A20/Abin-1$^{T-\Delta IEC}$Tnf$^{-/-}$* mice. For panels (**D**) and (**F**), significance was assessed by two-way ANOVA with Bonferroni's multiple comparison test. For panels (**E**) and (**G**), significance was assessed by Log-rank Mantel-Cox test. Only significant differences are shown; *=p<0.05, **=p<0.01, ***=p < 0.001; ****=p< 0.0001. Scale bars, 50μm. Data represent at least two independent experiments.
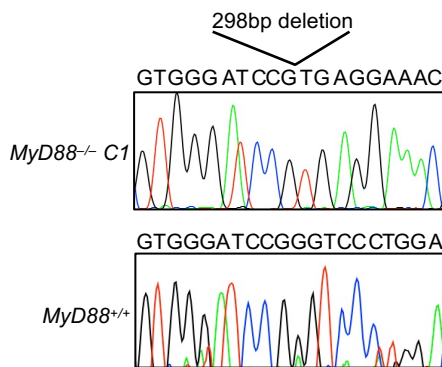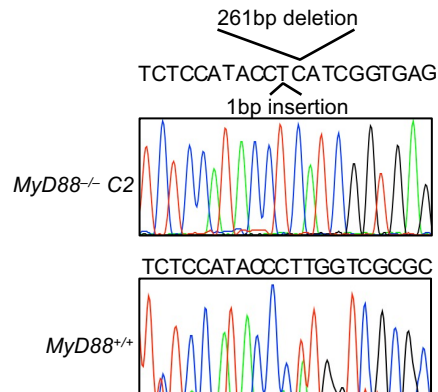
Supplemental Figure 1

Supplemental Figure 1. Tamoxifen-induced deletion of floxed A20 and ABIN-1 on a *Vil-cre-ER^T2+* background *in vivo* and *in vitro*.
(**A**) Immunoblotting analysis of IECs with the indicated genotypes 40h after treatment with 2mg tamoxifen *per os* (*p.o.*). (**B**) Immunoblotting analysis of *A20/Abin-1^T-ΔIEC^Tnf^-/-* enteroid cultures treated with the indicated concentration of 4-OHT for 24h. For panels (**A,B**), lysates were immunoblotted with the antibodies indicated on the right. (**C**) Representative confocal microscopy images of PI-stained enteroids from indicated genotypes of mice treated with vehicle or 4-OHT for 24h followed by 24 h of 2.5 ng/ml TNF as indicated. Scale bars, 100µm. (**D**) Quantitative luminescent cell viability assay of enteroid cultures treated as described in (**C**) (mean ± SEM). For panel (**D**), significance was assessed by two-way ANOVA with Dunnett's multiple comparison test comparing *A20/Abin-1^T-ΔIEC^* and *A20/Abin-1^T-ΔIEC^Tnf^-/-* to control *Vil-cre-ER^T2+* enteroids.
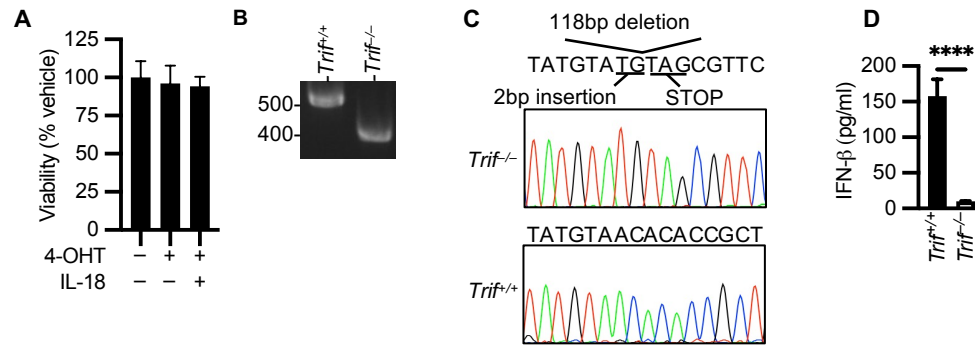
Supplemental Figure 2

Supplemental Figure 2. Editing of *MyD88* in *A20/Abin-1$^{T-ΔIEC}$Tnf$^{-/-}$* mice. Nucleotide chromatogram and sequence of the *MyD88* PCR amplicon surrounding the CRISPR-Cas9-targeted site for (**A**) *MyD88 C1* and (**B**) *MyD88 C2* in *A20/Abin-1$^{T-ΔIEC}$Tnf$^{-/-}$* mice.

Supplemental Figure 3

Supplemental Figure 3. IL18 stimulation of *A20/Abin-1$^{T-\Delta IEC}$Tnf$^{-/-}$* enteroids and editing of *Trif* in *A20/Abin-1$^{T-\Delta IEC}$Tnf$^{-/-}$* mice. (A) Quantitative luminescent cell viability assay of *A20/Abin-1$^{T-\Delta IEC}$Tnf$^{-/-}$* enteroid cultures treated with the indicated stimuli (mean ± SEM; IL-1β 25ng/ml). **(B)** Agarose gel electrophoresis and **(C)** nucleotide chromatogram and sequence of the *Trif* PCR amplicon surrounding the CRISPR-Cas9-targeted site in *Trif* for *A20/Abin-1$^{T-\Delta IEC}$Tnf$^{-/-}$* mice. **(D)** IFN-β ELISA of mouse splenocytes with the indicated genotype stimulated with 100 μg/ml poly(I:C). For panel **(A)** significance was assessed using one-way ANOVA with Dunnett's multiple comparison test relative to vehicle alone. For panel **(D)**, significance was assessed using unpaired t-test. Only significant differences are shown; ****=p< 0.0001. Data represent at least two independent experiments.

Supplemental Figure 4

Supplemental Figure 4. Deletion of *Casp8* in *A20/Abin-1$^{T-\Delta IEC}$Ripk3$^{-/-}$* mice and poly(I:C) stimulation of *A20/Abin-1$^{T-\Delta IEC}$Ripk3$^{-/-}$* and *A20/Abin-1$^{T-\Delta IEC}$Ripk3$^{-/-}$Casp8$^{-/-}$* enteroids. (**A**) Nucleotide chromatogram and sequence of the *Casp8* PCR amplicon surrounding the CRISPR-Cas9-targeted site in *Casp8* for *A20/Abin-1$^{T-\Delta IEC}$Ripk3$^{-/-}$* mice. (**B**) Immunoblot of intestinal epithelial cells from *A20/Abin-1$^{T-\Delta IEC}$Ripk3$^{-/-}$* mice with the indicated *Casp8* genotypes. (**C**) Quantitative luminescent cell viability assay of enteroids with the indicated genotype treated with indicated stimuli, (mean ± SEM). For panel (**C**) statistical significance was assessed by two-way ANOVA with Bonferroni's multiple comparison test comparing between genotypes for each stimulation condition. Only significant differences are shown; ***=p < 0.001; ****=p< 0.0001. Data represent at least two independent experiments.